(2)

Annual Report on

Investigations of Oxidation Protection Systems for Carbon-Carbon Composites Formed by Chemical Vapor Deposition and Plasma-Assisted Chemical Vapor Deposition Techniques

Prepared by
J. Don and M. A. Wright
(Principal Investigators)
and
Jun He

Report covers period 3/1/89 to 2/28/90
for
Air Force Office of Scientific Research/NE
Bolling Air Force Base
Washington, DC 20332-6448

Attn: L. J. Schioler

REPORT DOCUMENTATION PAGE

Form Approved
OMB No. 0704-0188

1. AGENCY USE ONLY (Leave blank)	2. REPORT DATE	3. REPORT TYPE AND DATES COVERED
	1991/1/21	INTERIM 1 Mar 89 - 30 Nov 90

4. TITLE AND SUBTITLE OXIDATION PROTECTION SYSTEMS FOR CARBON-CARBON COMPOSITE FORMED BY CHEMICAL VAPOR AND DEPOSITION AND PLASMA ASSISTED CHEMICAL VAPOR DEPOSITION TECHNIQUES

5. FUNDING NUMBERS
GRANT
AFOSR-88-0130

6. AUTHOR(S)
J. DON, J. HE, M.A. WRIGHT

7. PERFORMING ORGANIZATION NAME(S) AND ADDRESS(ES)
SOUTHERN ILLINOIS UNIVERSITY AT CARBONDALE
CARBONDALE ILLINOIS 62901

8. PERFORMING ORGANIZATION REPORT NUMBER
AFOSR-2.

9. SPONSORING / MONITORING AGENCY NAME(S) AND ADDRESS(ES)
AIRFORCE OFFICE OF SCIENTIFIC RESESRCH
BOLLING AIRFORCE BASE
WASHINGTON, DC, 20332-6448.

10. SPONSORING / MONITORING AGENCY REPORT NUMBER
2306/A2

11. SUPPLEMENTARY NOTES

12a. DISTRIBUTION / AVAILABILITY STATEMENT
UNCLASSIFIED/UNLIMITED.

12b. DISTRIBUTION CODE
UNCLASSIFIED.

13. ABSTRACT *(Maximum 200 words)*

Conditions necessary for the preparation of pack cemented oxidation resistant reacted layers on carbon-carbon composites were developed. Reacted layers were produced containing SrC, ZrC, B4C. The oxidation resistance of such layers were listed in air at temperatures up to 1800°C and the results were compared. Additional surface layers deposited into the reacted layers consisted of SiC, ZrB2, SiC/Zrb2 and graded Sic/ZrC. These layers significantly improved the oxidation resistance of the layers generated by pack cementation the oxidation resistance of the combined layer systems (pack cementation plus CVD) was determined by subjecting each system to an air environmental in an isothermal and a cyclicly varying temperature environmental temperatures up to 1700°c.

14. SUBJECT TERMS	15. NUMBER OF PAGES
OXIDATION RESISTANCE, CHEMICAL VAPOR DEPOSITION, CARBON CARBON	16. PRICE CODE

17. SECURITY CLASSIFICATION OF REPORT	18. SECURITY CLASSIFICATION OF THIS PAGE	19. SECURITY CLASSIFICATION OF ABSTRACT	20. LIMITATION OF ABSTRACT
UNCLASSIFIED	UNCLASSIFIED	UNCLASSIFIED	

TABLE OF CONTENTS

List of Figures

INTRODUCTION

Carbon materials reinforced with carbon fibers, otherwise known as carbon-carbon (C-C) composites, offer many advantages over traditional materials. Primarily, their large strength-to-weight ratio, and the retention of strength at high temperatures make C-C composites extremely attractive high temperature, structural materials.

While the strength of the superalloys and ceramic composites decreases with increasing temperature, the strength of C-C composites slightly increases at temperatures well above the maximum usage temperatures of other materials. The fact that C-C composites exhibit low density and are able to maintain room temperature strengths at temperatures above 2225°C[1] has far reaching applications, especially for the aircraft and aerospace industries. Unfortunately, C-C composites undergo severe oxidation when exposed to oxidizing environments at temperatures above 370°C.[2] Thus, methods to prevent gasification must be developed if C-C composites are to develop their full potential.

A successful oxidation-protection system should meet four main requirements: adequate adhesion between substrate and coating; maximum resistance to thermal shock and thermal cycling; good oxidation protection at both intermediate (1000°C) and high (>1500°C) temperatures; and good substrate oxidation resistance at moderate temperatures.

The objective of this investigation was to develop effective high temperature coatings capable of providing oxidation resistance for carbon-carbon composites. Two types of coating were investigated; a simple pack cementation conversion coating [3-6] and

a duplex coating consisting of a conversion coating onto which an additional layer was applied by Chemical Vapor Deposition.[7-9] A computer-controlled CVD reactor was specifically designed and constructed for this program. The oxidation protective coatings formed using the pack cementation technique produced conversion coatings of: (1) SiC, (2) SiC with B_4C, and (3) SiC with ZrC. These coatings were characterized and the oxidation resistance was measured and reported. Four types of CVD coating systems were investigated. They were SiC monolayer, ZrB_2 monolayer, ZrB_2/SiC multilayer and graded ZrC/SiC coatings. Following these coating experiments, the characterization of the microstructures was performed and the degree of oxidation protection was determined. The CVD reactor and the oxidation testing equipment were all computer-controlled and were designed and constructed for this program. Detailed microstructural analysis was also performed using optical microscopy, scanning electron microscopy, transmission electron microscopy, and x-ray diffraction.

Papers Presented

Two papers were presented at "The 14th Conference on Metal Matrix, Carbon and Ceramic Matrix Composites," NASA/DOD joint conference, Cocoa Beach, Florida, January 17-19, 1990. These are included as addenda to this report and are entitled "Microstructure of Pack Cemented SiC Protective Coatings for Carbon-Carbon Composites" and "Isothermal and Cycled Oxidation Resistance of Ceramic Coated Carbon-Carbon Composites."

Experimental Procedures

Pack Cementation

Different pack cementation mixtures were used to study the effects of additions to the oxidation resistant coatings that were produced. Essentially, either ZrC or B_4C was added to the basic conversion coating of SiC. In addition, Al_2O_3 was added to some pack mixtures.

In general, Al_2O_3 in the starting pack composition produced the following effects on the conversion layers that were produced.

i) In the SiC/Si system, Al_2O_3 decreased the conversion layer thickness and decreased the amount of free silicon (Si) in the conversion layer.

ii) In the ZrC/SiC/Si system, Al_2O_3 increased the conversion layer thickness and decreased the amount of ZrC dispersed in the conversion layer.

iii) In the ZrC/SiC/B system, Al_2O_3 increased the conversion layer thickness and increased the amount of B_4C dispersed in the conversion layer.

The powders used for the pack cementation process were a weight percent mixture of silicon (Si), silicon carbide (SiC), zirconium carbide (ZrC), Boron (B), and Alumina (Al_20_3). The time and temperature used for the pack cementation process were varied and depended on the both the desired thickness of the converted layer and the composition of the powder mixture to be used. Pack powder mixtures containing ZrC were held at 1900°C for five hours. Compositions without ZrC were held at 1700°C for three hours.

Based on preliminary results of pack cementation and x-ray diffraction

experiments, the powder mixtures and the optimized processing conditions listed in Table 1 were used for this study.

TABLE 1
THE POWDER MIXTURES OF PACK CEMENTATION EXPERIMENTS

PACK COMPOSITION (% by weight)	TEMPERATURE (°C)	TIME (Hr)
66 SiC/33 Si	1700	3
60 SiC/30 Si/10 Al_2O_3	1700	3
30 ZrC/30 SiC/40 Si	1900	5
30 ZrC/30 SiC/30 Si/10 Al_2O_3	1900	5
30 ZrC/30 SiC/40 B	1900	5
30 ZrC/30 SiC/30 B/10 Al_2O_3	1900	5

Chemical Vapor Deposition (CVD)

The coating systems investigated in this study were SiC, ZrB_2, SiC/ZrB_2 multilayer coating, and SiC/ZrC graded coating. Table 2 summarizes the gas precursors used for these coatings.

TABLE 2
CVD GAS PRECURSORS AND THE ASSOCIATED CHEMICAL REACTIONS

Coating	Raw Materials	Chemical Reaction
SiC	CH_4, SiH_4, H_2	$CH_4 + SiH_4 = SiC + 4H_2$
ZrB_2	$ZrCl_4$, BCl_3, H_2, Ar	$ZrCl_4 + 2H_2 = Zr + 4HCl$ $2BCl_3 + 3H_2 = 2B + 6HCl$ $Zr + 2B = ZrB_2$
SiC + ZrB_2	CH_4, SiH_4, H_2 $ZrCl_4$, BCl_3, Ar	All reactions above are involved.
SiC + ZrC	CH_4, SiH_4, H_2 $ZrCl_4$, Ar	$CH_4 + SiH_4 = SiC + 4H_2$ $CH_4 + ZrCl_4 = ZrC + HCl$

(1) SiC Coating

The optimum CVD deposition temperature was found to be about 1200°C. At this temperature, a fine polycrystalline SiC coating that exhibited, good adhesion between coating and substrate and proper coating thickness was obtained. A smooth, pure SiC coating layer was found to be deposited at 2 torrs of pressure and an SiH_4/CH_4 ratio of 1:3.

(2) ZrB_2 Coating

As noted in Table 2, the source gases used for the ZrB_2 coating experiments were $ZrCl_4$, BCl_3 and H_2. In order to introduce the $ZrCl_4$ vapor into the reaction chamber, Ar was used as a carrier gas. Based on preliminary test runs, it was found that an Ar/BCl_3 ratio of 2:1 produces a pure ZrB_2 coating. Since chlorides were used as the primary source gases, a large amount of excess H_2 was needed to reduce the chlorine gases. A series of test runs showed that a ZrB_2 coating could be deposited using 30 sccm of Ar, 15 sccm of Bcl_3, and 420 sccm of H_2 at 1300°C and 10 torrs of pressure.

(3) SiC and ZrB_2 Multilayer Coating

The source gases for this deposit is also shown in Table 2. A pure ZrB_2 coating forms borate glass during oxidation at temperatures much lower than those required to form a molten silicate from a SiC coating. However, vaporization of the borate occurs as the temperature is raised and protection is lost. In order to retard the vaporization of the borate glass, a SiC over coat was applied on top of the ZrB_2 coating. The ZrB_2 inner layer and an SiC overcoat were deposited using the parameters described earlier in this section.

(4) SiC and ZrC Graded Coating

In order to obtain graded coatings, flow rates of H_2 and CH_4 were kept constant throughout the entire experiment. Conversely, the flow rate of $ZrCl_4$, which was carried by the Ar carrier gas, was initially fast, while the flow rate of SiH_2 was slow. This produced a coating predominantly ZrC. After some time, the flow of argon was gradually reduced to zero (to produce a layer containing increasing amounts of SiC) before being increased to produce a predominantly ZrC final layer. With this type of flow control, it has been demonstrated that CVD experiments performed at 1300°C, 1.5 torr yielded the desired graded coating of SiC and ZrC.

Results

Pack Cemented Coatings:

X-ray diffraction was used to characterize the composition of conversion layers. The results are listed in Table 3.

TABLE 3

X-RAY DIFFRACTION RESULTS OF THE PACK CEMENTED COATINGS

PACK COMPOSITION (% by weight)	CONVERSION LAYER COMPOSITION*
66 SiC/33 Si	SiC + Si**
60 SiC/30 Si/10 Al_2O_3	SiC + Al mixture
30 ZrC/30 SiC/40 Si	SiC + ZrC + SiC**
30 ZrC/30 SiC/30 Si/10 Al_2O_3	SiC + Al mix + ZrC + $ZrSi_2$
30 ZrC/30 SiC/40 B	SiC + B_4C + ZrB_2** + SiC**
30 ZrC/30 SiC/30 B/10 Al_2O_3	B_4C + SiC + SiC + ZrB_2 + Al mix

Oxidation Resistance

The pack cementation process usually produced a converted layer that was relatively inhomogeneous and was porous. Thus, some variability in the oxidation resistance was observed.

Test Conducted at 800°C

The percent weight change with time exhibited by each of the compositions exposed to 800°C in air, are shown in Figure 1. It was found that coatings consisting of SiC with B_4C provided the best oxidation protection at this temperature. In this coating system, the surfaces, as examined by SEM, were covered with copious amounts of a glassy layer, whereas only limited amounts of glass were formed in either of the other systems. At 800°C, SiC coatings which contained ZrC exhibited the poorest oxidation protection of all the coatings investigated.

Tests Conducted at 1000°C

The overall weight change exhibited by specimens exposed to 1000°C are shown in Figure 2, given in percent weight change as a function of time. At this temperature, the vapor pressure and hence the volatilization rate of B_2O_3 increases. Thus, the oxidation protection provided by the coatings of SiC and B_4C decreases from that provided at 800°C. In contrast, elemental SiC, which is essentially unreactive at 800%C, oxidizes at 1000°C to form a SiO_2 glass that is able to slowly flow and seal the cracks in the SiC coating. As a result, SiC provided better protection against oxidation at 1000°C than at 800°C. Similar to the case found at 800°C, coatings of SiC and ZrC were not better than elemental SiC in providing oxidation protection at 1000°C, as indicated in Figure 2.

Tests Conducted at 1800°C

Specimens of each composition were also subjected to an air environment at 1800°C. The weight changes are presented in Figure 3. At 1800°C, the duplex SiC + B_4C coatings quickly volatilize, leaving the surface of the composite open to rapid oxidation. However, contrary to tests carried out at low temperatures, the SiC + ZrC coatings provided good protection at high temperature. This probably resulted from the increased conversion layer thickness. Significant bubble formation was observed in this coating, however, this did not seem to deleteriously effect the oxidation resistance since the surface of the composite was completely covered with a glassy film. In contrast to observations made on other specimens, spalling of this coating and exposure of the carbon-carbon surface did not occur.

Summary of Oxidation Tests of the Pack-Cemented Carbon-Carbon

Figure 4 shows the oxidation results of pack cemented SiC + B_4C coatings obtained without using Al_2O_3 in the reactive mixtures. The best protection available with this coating occurred at 800°C, where the low viscosity borate glass was able to flow and seal the surface cracks. The protection offered by this coating decreased with increasing temperature because, above 1000°C the vapor pressure of B_2O_3 becomes too high to provide much protection. As the temperature increases, the vapor pressure increases, providing less and less protection.

When Al_2O_3 is added to the reactive mixture of SiC + B_4C used to produce the pack cemented coating, the thickness of the conversion layer produced in a given time increases. And, the protection provided by the coating was better at all the test

temperatures than that obtained without Al_2O_3. This superiority is noted by comparing the results of Figure 4 and Figure 5. The increase in protection is due both to the increase in thickness of the conversion layer and to the formation of significant amounts of borosilicate glass during the conversion process.

The change in weight of carbon-carbon protected with SiC coatings produced from SiC + Al_2O_3 reactive powder is shown over an extensive temperature range in Figure 6. SiC coatings offer their best protection around 1200°C. As can be inferred from thermodynamic considerations, the SiC readily oxidizes to form a SiO_2 glass film at temperatures of about 1200°C. This film flows easily at this temperature and can easily seal defects in the SiC coating, i.e., cracks. The easy flow characteristics of SiO_2 are also exhibited at 1400°C, however, the vapor pressures of the products of oxidized SiC in the presence of carbon, primarily CO, as well as SiO, and SiO_2 become significant at these temperatures and this gas evolution adversely effects the protection offered by the SiC layer.

Although the glassy SiO_2 sealant film forms around 950°C and begins to flow around 1000°C, the glass is quite viscous; thus, crack sealing usually takes place slowly and usually occurs only after significant oxidation of the carbon has occurred. This is the reason why SiC coatings do not protect efficiently at temperatures below 1000°C. In addition, at 800°C, SiC does not oxidize readily to form SiO_2 glass. Since crack sealing will not occur in the absence of a viscous glass, SiC alone is not able to provide adequate protection at this temperature.

At 1600°C and above, SiO_2 tends to dissociate. The vapor pressures SiO_2 over

SiC and carbon become large and tend to disrupt the continuity of the protective film. Therefore, less protection is provided at these temperatures than at the 1200-1400°C range, as shown by the very large weight losses recorded for oxidized specimens in Figure 6.

At lower temperatures, the SiC + ZrC coatings are not expected to provide noteworthy oxidation protection, since the SiC is not able to form a protective glass at lower temperatures and ZrC forms an unprotective oxide.

At the intermediate temperatures, the SiC portion of the coating oxidizes to form a protective seal. ZrO_2 may react with the SiO_2 film to form zirconium silicate, which offers reasonable oxidation protection.

Although the SiC + ZrC coating oxidizes quickly at the high temperatures tested, it does appear that the ZrC additions improve the oxidation resistance of the SiC coating. This is possibly due to the reducing effect ZrC has on the vapor pressures of the silicon system, through the formation of the zirconium silicide and zirconium silicate.

External CVD Coatings

In this investigation, the following external CVD coatings were produced: SiC, ZrB_2, SiC/ZrB_2 multilayer coating and SiC/ZrC graded coating. Results of CVD experiments, microstructural studies, and oxidation tests for these coatings are presented below.

SiC Coating

It was found that the deposition rates at 1000°C were very slow and that the SiC coatings obtained were too thin to be capable of protecting the substrate. On the other

hand, deposition temperatures above 1400°C generated enough internal stress to cause the coating to spall during cool down. The optimum temperature range for the production of continuous oxidation resistant coatings was found to be between 1200 and 1250°C. The coating deposited at this temperature consisted of fine polycrystalline grains. Its adhesion to the substrate and the deposition rate were both satisfactory.

The flow rate ratio of SiH_4 to CH_4 had a great effect on the final coating composition. Figure 7 shows typical gas flow rate curves for depositing silicon carbide and Figure 8 is an X-Ray diffraction pattern of the SiC coating obtained. In addition to the predominant phase of SiC, a small amount of free Si were also found in the coating. The two phase mixture (light and dark phases) can be observed in Figure 9. The micro-hardness value of this coating was approximately 2700 kg/mm^2 on the knoop scale, which is consistent with the reported micro-hardness value of CVD silicon carbide. Good bonding between the pack cemented substrate and the CVD coating was also observed.

Isothermal and thermally cycled oxidation tests were conducted on SiC-coated carbon-carbon specimens obtained by using CVD gas flow rates shown in Figure 7. Figure 10 is a TGA thermogram of the isothermal oxidation tests carried out in air at 1500° and 1700°C. After 10 hours, the specimen oxidized at 1500°C gained 3.5% of its initial weight whereas the specimen oxidized at 1700°C showed less than 1% weight gain. Figure 11 compares the results of the isothermal test and the thermal cycling test at 1700°C. In the thermal cycling test, the oxidation temperature was cycled between room temperature and 1700°C, with a residence time of 0.5 hour at 1700°C and a 3-minute resting period between each cycle. The thermal cycling test showed no significant weight

change in the initial seven cycles. After 10 hours of the cycling test, the specimen showed about 4.4% weight loss. The weight loss during the thermal cycling test was a linear function of time, which indicated that the oxidation was reaction-controlled.

Figure 12 is an SEM photograph of a SiC-coated specimen oxidized at 1500°C. No significant damage of the coating was found after the oxidation. However, oxidation at 1700°C caused bubble formation on the same coated specimen within a short period of time. As shown in Figure 13, bubbling was observed after three hours of oxidation at 1700°C.

ZrB_2 Coating

In addition to the compounds of silicon, such as the glass formers of SiC and Si_3N_4, metal diborides have also been reported to be good candidates for oxidation protection. ZrB_2 was selected in this study because it tends to form a borate glass at high temperatures. Figure 14 shows a experimental gas flow rate pattern of the ZrB_2 deposition. After a series of test runs, it was found that the optimum condition for depositing ZrB_2 was: 1300°C, 30 sccm of Ar (as a $ZrCl_4$ carrier gas), 15 sccm of BCl_3, 420 sccm of H_2, and 10 torrs of pressure.

An X-Ray diffraction spectrum of a ZrB_2 coating obtained by using the coating conditions described above is shown in Figure 15. The diffraction pattern shows that the predominant phase in the coating is ZrB_2, along with a small amount of B_4C. Figure 16 is an optical micrograph of this ZrB_2 coating, which shows very good adhesion between the coating and the carbon substrate. However, the number of thermal cracks was found to be higher than in the case of the SiC coating. This is because that the CTE of ZrB_2

(4.6×10^{-6} °C^{-1}) is much larger than the CTE of SiC (3.6×10^{-6}°C^{-1}).

Although ZrB_2 is quite refractory, the oxidation results of ZrB_2 coatings were not encouraging. During the oxidation, the ZrB_2-coated specimen started to smoke badly at about 1000°C and suffered severe weight loss when the temperature reached 1500°C. The oxidized specimen surface was partially covered with a white powdery residue. Analysis result showed that the residue was predominantly ZrO_2 and the X-ray diffraction spectrum is shown in Figure 17.

In order to find out how and why ZrB_2 fails to protect carbon-carbon composites, an oxidation test was interrupted after 10 minutes and the oxidized specimen was examined by SEM. As shown in Figure 18, it was found that the glass sealant of B_2O_3 bubbled and ruptured during the oxidation, leaving a particulate residue, presumably ZrO_2, in the holes where the bubbles ruptured. The remaining B_2O_3 glass, i.e., the background phase in Figure 18, also started to degrade. Micro-cracks began to develop as the vaporization of B_2O_3 continued in order to release the pressure build-up due to the formation of new bubbles. Eventually, the structure of the ZrO_2 residue shown in Figure 19 resulted. The events occurred during the oxidation of the ZrB_2 coating indicated that Zr was not involved in forming a passive Zr-containing borate glass. The oxidation reaction of ZrB_2 seemed to be:

$$ZrB_2 + 5/2\ O_2 \rightarrow ZrO_2 + B_2O_3 \qquad \text{Eq. 4-16}$$

The B_2O_3 product was vaporized quickly since its melting point is only 449°C.

Although the oxidation protection capability of the ZrB_2 coatings was not

established, it is interesting to note that this coating may help to improve the oxidation protection of carbon-carbon composites at intermediate temperatures, since it forms B_2O_3 glass at a temperature lower than 1000°C. Therefore, if ZrB_2 is used in conjunction with a SiC coating, low viscosity borate glass might be formed which would provide protection at low temperatures. Thus, better thermal cycling properties should be expected.

SiC and ZrB_2 Multilayer Coating

The multilayer coating of SiC + ZrB_2 consisted of an inner layer of ZrB_2 and an overcoat of SiC. As described in the previous paragraph, this composite coating was expected to offer good oxidation protection at both intermediate and high temperatures.

The conditions for obtaining the multilayer coating were adopted from the previous SiC and ZrB_2 CVD experiments. Three hours of SiC coating were followed by another three hours of ZrB_2 deposition in order to form the desired multilayer coating.

Since efficient protection over an extensive cyclic temperature range was expected when using this multilayer approach, the thermal cycling test was of primary interest in this study. In particular, since oxidation at 1000°C is expected to be significant, due to the high viscosity of the SiO_2 glass formed from SiC and, since 1500°C is the maximum temperature that a carbon-carbon composite coated with SiC would experience, a 2-stage thermal cycling procedure was used which included residence time periods at both 1000°C and 1500°C. Figure 20 illustrates the weight loss experienced by C-C subjected to 16 cycles of the 2-stage thermal cycling test performed on a multilayer-coated composite. As shown in Figure 20, the temperature was increased from room

temperature to 1000°C in two minutes and remained at the temperature for half an hour. The temperature was then increased to 1500°C in one minute before being held for another half hour. It was then cooled to room temperature in a further two minutes. After 25 hours of testing, the specimen showed a uniform, reflective, glassy surface without any trace of damage due to oxidation. The total weight loss of the specimen was less than 1%. SEM observations showed that a few chipped areas caused by prior CVD cool down were all perfectly covered with glass (Figure 21). Apparently, glass flowed efficiently at 1000°C and remained stable at 1500°C. It indicated that B_2O_3 and SiO_2 reacted readily, leading the formation of borosilicate glass which provided good protection over a wide temperature range. Additionally, no evidence of ZrO_2 was found. This implies that Zr was contained in the glass and it may have offered an advantageous effect to the glass.

SiC and ZrC Graded Coating

Figure 22 shows the graded coating obtained by controlling gas flow rates according to the flow rate curves shown in Figure 23. As shown in the micrograph, the fraction of fine SiC grains gradually increases as the layer thickness increases. It appears that the use of low SiH_4/CH_4 and high $ZrCl_4/CH_4$ flow rate ratios yielded a fine-grained two phase mixture of ZrC and SiC.

Isothermal oxidation tests at 1500°C in air were performed on a specimen obtained by using the gas flow rates shown in Figure 23. After 10 hours the specimen showed no weight loss. Instead, a weight gain of 1% was observed. The SEM micrograph (Figure 24) shows that the surface of the oxidized specimen contained a two

phase mixture of SiO_2 glass and a fine crystalline phase, presumably a zirconium-containing silicate.

Figure 25 shows the control of gas flow rates which proved to be the best of the flow rate conditions for SiC/ZrC graded deposition. An oxidation test performed on the coated specimen obtained showed no appreciable weight loss after 100 hours of testing at 1500°C in air. The TGA result is shown in Figure 26, as compared with the oxidation of pack-cemented specimens.

Oxidation tests at 1700°C were also performed on this type of coated specimen. After 10 hours of oxidation at 1700°C, the specimen showed no evidence of damage, as shown in Figure 27. The coating gradually degraded after prolonged oxidation at 1700°C. As seen in Figure 28, after 21 hours of oxidation, moderate bubbling occurred; however, no evidence of appreciable damage on the surface was observed.

Figure 29 is a TEM bright field image of the surface glass formed during oxidation. The associated selecting area diffraction (SAD) pattern is shown in Figure 30. It is evident that the glass also contained small crystals which were 0.01 - 0.02 microns in size. The SAD pattern, along with X-ray diffraction pattern of Figure 31, proved that these tiny crystals were $ZrSiO_4$. Although the viscosity and the structure of the glassy phase are yet to be investigated, the morphology of the glass layer seemed to indicate that the protective surface layer is capable of providing a reasonable resistance to both oxygen diffusion and erosion.

CONCLUSIONS

1. Starting pack compositions consisting of 30%ZrC-30%SiC-40%Si and 30%ZrC-

30%SiC-40%B result in conversion coating compositions of SiC + ZrC and SiC + B4C, respectively, when heated to 1900°C for 5 hours.

2. Al_2O_3, in the starting pack composition, has the following effects on the conversion layers of the pack compositions listed below.

   i. In the SiC/Si system, Al_2O_3 decreases the conversion layer thickness and decreases the amount of free Si in the conversion layer.

   ii. In the ZrC/SiC/Si system, Al_2O_3 increases the conversion layer thickness and decreases the amount of ZrC dispersed in the conversion layer.

   iii. In the ZrC/SiC/B system, Al_2O_3, increases the conversion layer thickness and increases the amount of B_4C dispersed in the conversion layer.

3. For the oxidation protection of C-C composites between 800-1000°C, SiC containing B_4C conversion layers provide the best protection; between 1200-1400°C, SiC conversion layers provide the best protection; and between 1600-1800°C, SiC containing ZrC provides the best protection.

4. Thermochemical calculations performed using a modified SOLGASMIX program were consistent to certain degrees with experimental results.

For obtaining the SiC coating, the flow rate ratio of CH_4/SiH_4 should be slightly larger than 1 and smaller than 4. 20 sccm of Ar as a carrier gas for $ZrCl_4$, 40 sccm of Bcl_3, and 500 sccm of H_2 were used to produce the ZrB_2 coating. For the ZrC coating, 60 sccm of Ar and 40 sccm of CH_4 were found to be successful.

5. The SiC coating protected carbon-carbon composites against oxidation at 1500°C and 1700°C for 10 hours without any weight loss in isothermal tests. The thermal cycling

test at 1700°C showed no significant weight change in first 8 cycles, and 4.4% weight loss in the next 8 cycles. These results indicate that SiC coating is capable of protecting the carbon-carbon substrate in a oxidizing atmosphere up to 1700°C.

6. ZrB_2 coating can not protect carbon-carbon substrate from oxidation at 1500°C. It formed a low melting point, high vapor pressure boron oxide glass, which evaporated at the testing temperature and destroyed the coating layer because of bubbling and spallation.

7. ZrB_2/SiC multilayer coating greatly improved the oxidation resistance of carbon-carbon composites at both intermediate (1000°C) and high temperatures (1500°C). The thermal cycling test showed that this coating formed low viscosity glass at a temperature lower than 1000°C. The glass sealed off cracks and spalled areas during oxidation. SiC and ZrB_2 together formed borosilicate glass which also protected the carbon-carbon substrate from oxidation at higher temperatures.

8. Graded Coating System

A graded ZrC and SiC coating with fine-grained structure offers good oxidation protection for carbon-carbon composites because it enhances both chemical and mechanical stabilities. A gradual transition from ZrC to SiC reduces the chance of interface delamination, while a fine, polycrystalline structure is more resistant to thermal cracking as compared to a coarse, columnar coating. This graded coating survived a 100-hour isothermal oxidation test in air at 1500°C with only a 0.61% weight loss. An isothermal oxidation test at higher temperature, 1700°C, shows less than a 1% weight loss after 21 hours. A glass phase as well as zirconium silicate were identified by

microscopy study. No evidence of appreciable damage of the coating or gasification of the carbon-carbon substrate was observed.

REFERENCES

1. J. Buckley, "**Carbon-Carbon, An Overview**," Am. Ceram. Soc. Bull., 67 (2) pp. 364-368, 1988.

2. J. Strife and J. Sheehan, "**Ceramic Coatings for Carbon-Carbon Composites**," Am. Ceramic. Soc. Bull., 67 (2) pp. 369-374, 1988.

3. D. C. Rogers, D. M. Shuford and J. I. Mueller, "**Formation Mechanism of a Silicon Carbide Coating for a Reinforced Carbon-Carbon Composite**," Proceedings of the 7th National SAMPE Technical Conference, pp. 319-336, 1975.

4. D. C. Rogers, R. O. Scott and D. M. Shuford, "**Material Development Aspects of an Oxidation Protection System for a Reinforced Carbon-Carbon Composite**," Proceedings of the 8th National SAMPE Technical Conference, pp. 308-336, 1976.

5. D. Shuford, U.S. Patent # 4,465,777 (August 1984 to Vought Corp.).

6. D. Shuford, U.S. Patent # 4,471,023 (September 1984 to Vought Corp.).

7. J. E. Sheehan, "**Ceramic Coatings for Carbon Materials**," Proceedings of the 4th Annual Materials Technology Center Conference on Recent Research into Carbon Composites, SIUC, pp. 369-374, 1987.

8. R. A. Rapp and G. R. St. Pierre, "**New Options for the Protection of Carbon/Carbon Composites**," presented at the High Temperature Composites Initiative Materials Compatibility Meeting, Dayton, Ohio, Oct. 1985.

9. G. H. Schiroky, J. L. Daae and J. E. Sheehan, "**High Temperature Oxidation of CVD Silicon Carbide**," Proceeding of the 87th Annual Meeting of the American Ceramic Society, May 1985.

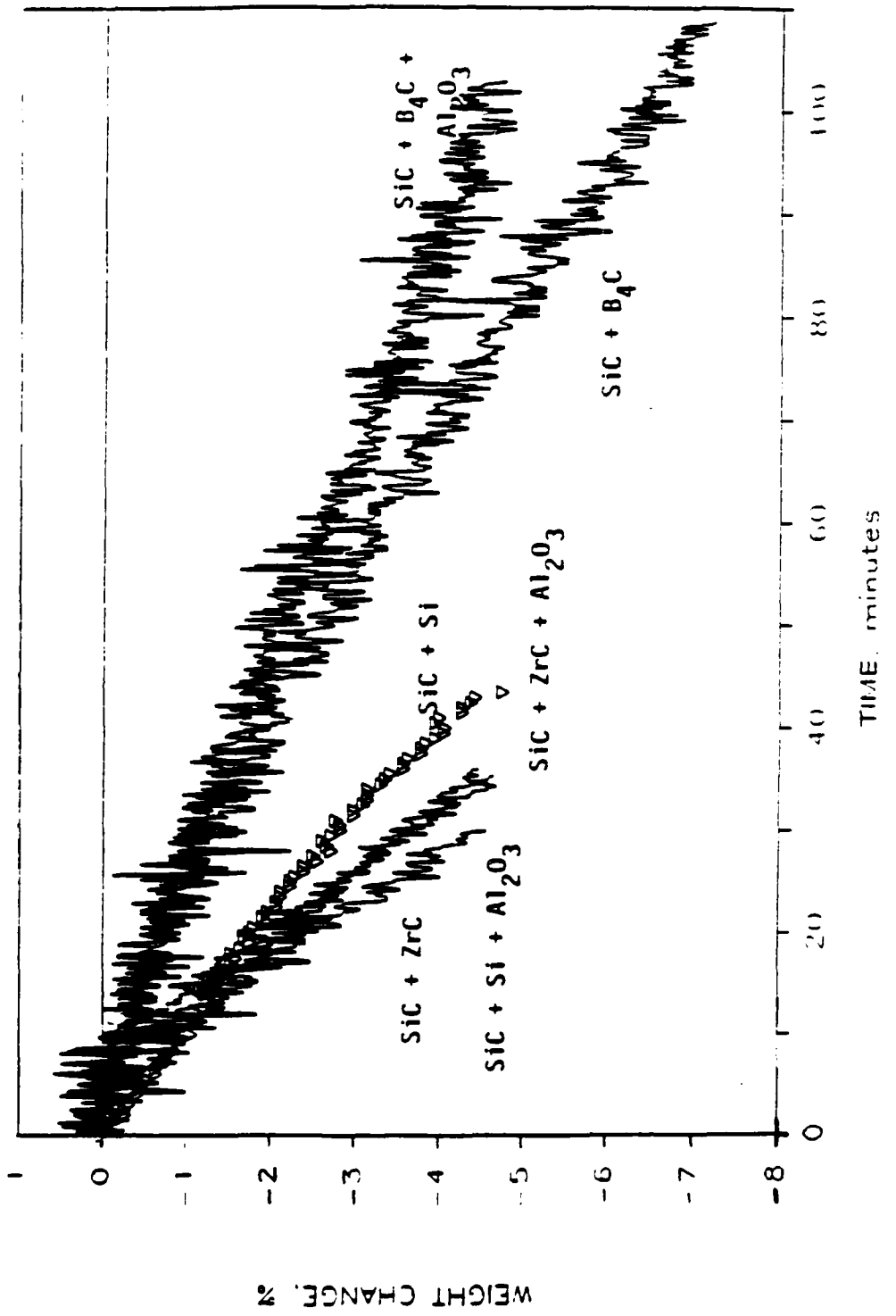

Figure 1. Comparison of Oxidation Results for All Mixtures Tested at 800°C.

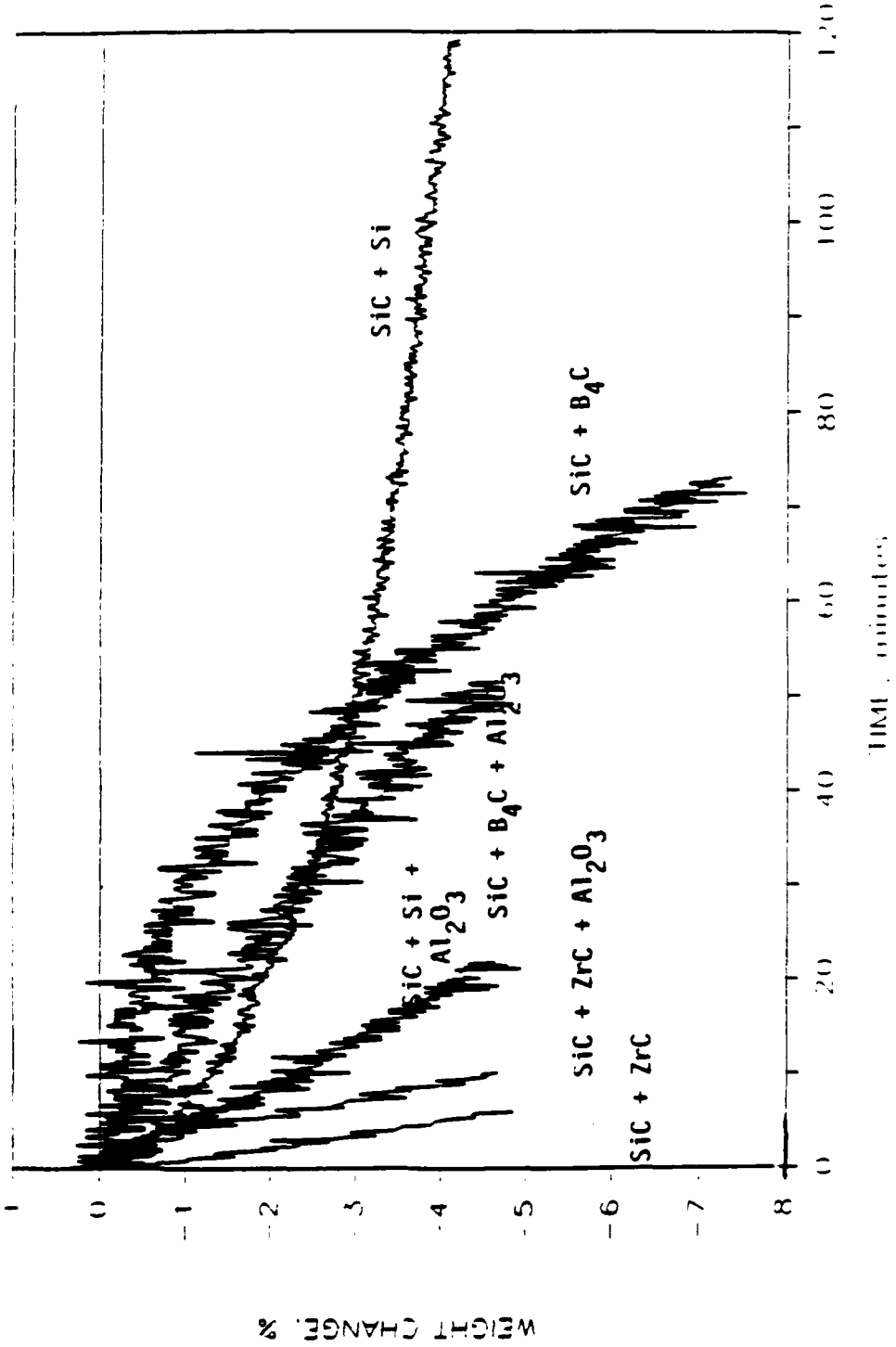

Figure 2. Comparison of Oxidation Results for All Mixtures Tested at 1000°C.

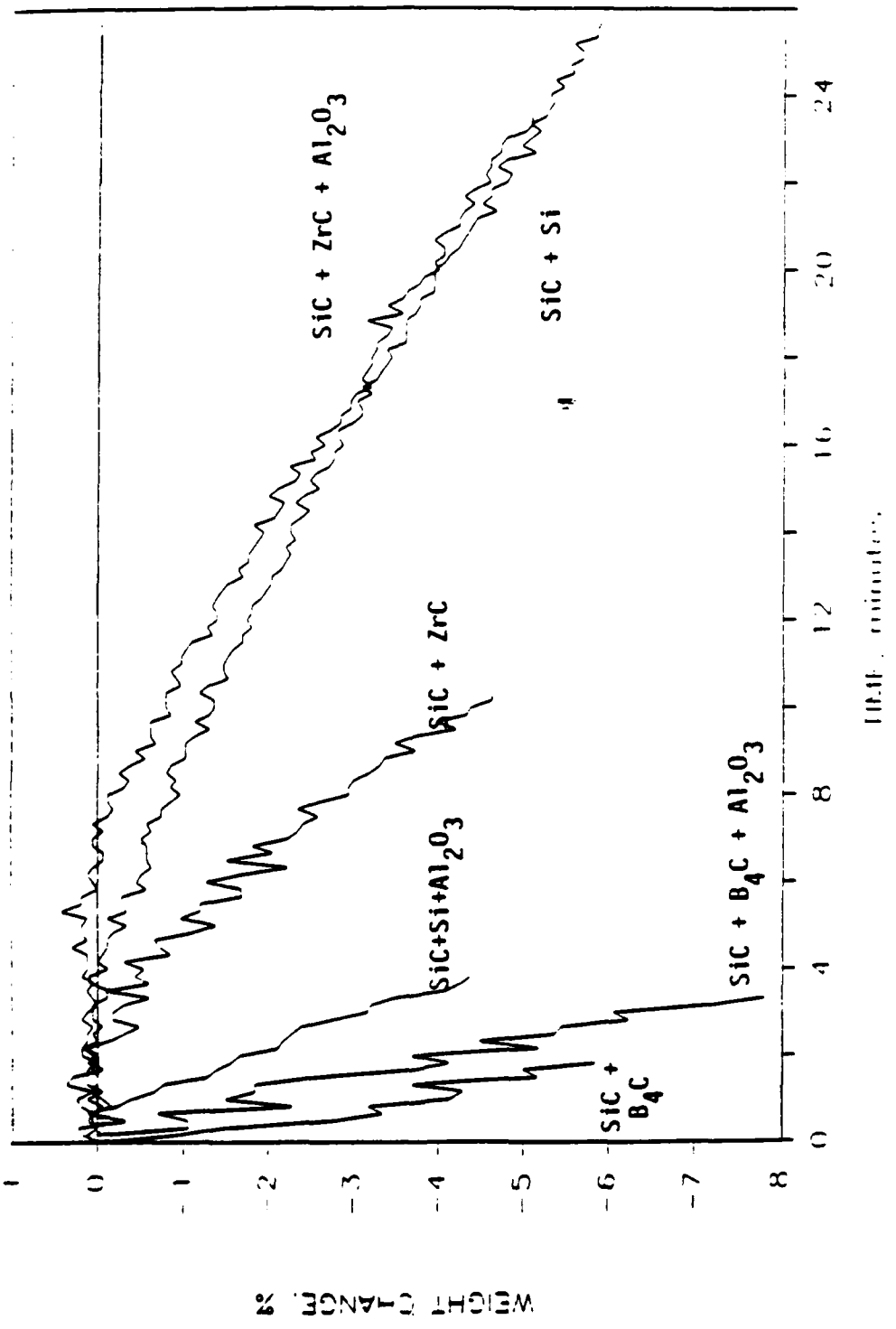

Figure 3. Comparison of Oxidation Results for All Mixtures Tested at 1800°C.

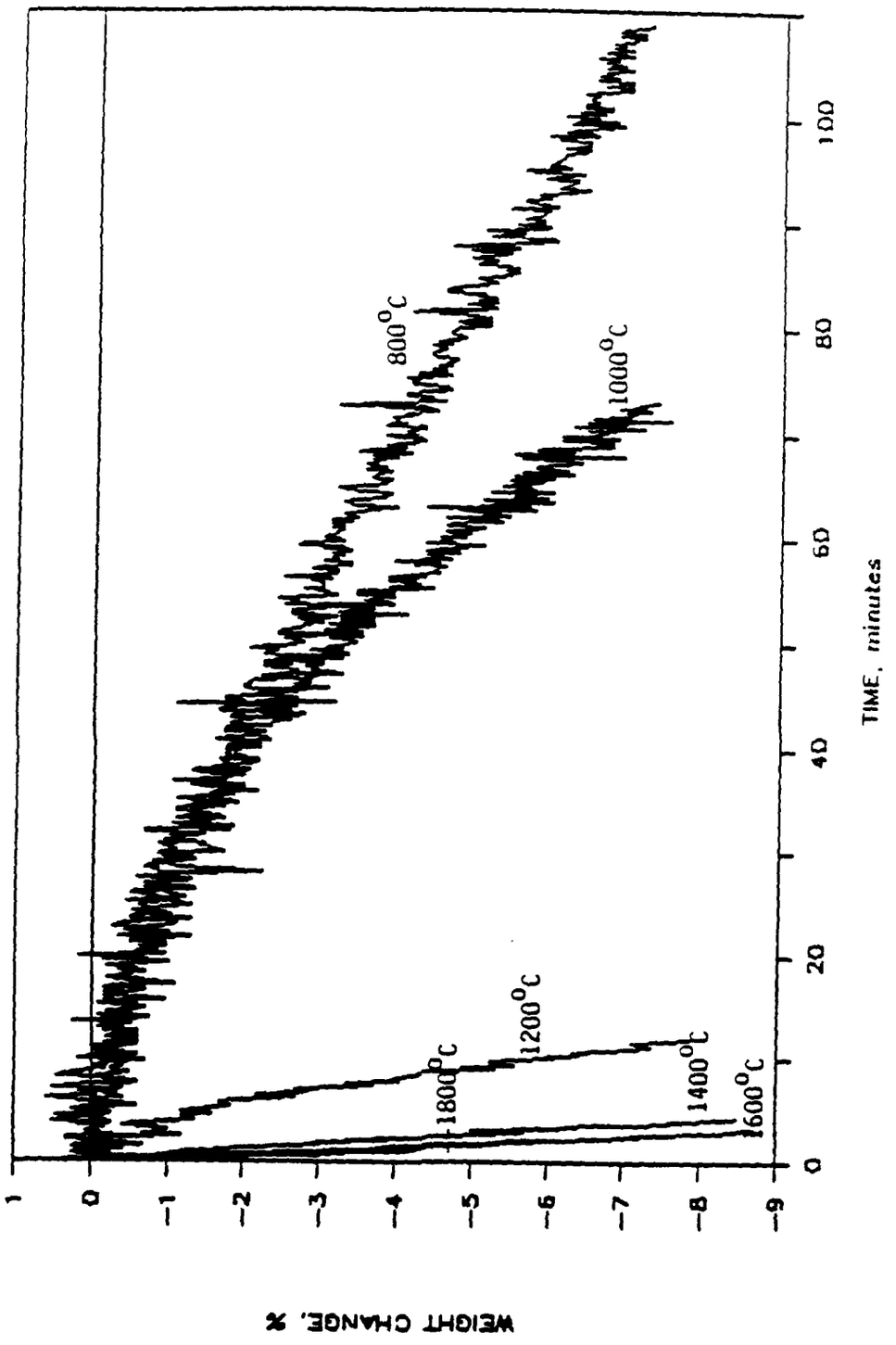

Figure 4. Oxidation Results at All Temperatures for the SiC + B_4C Coating.

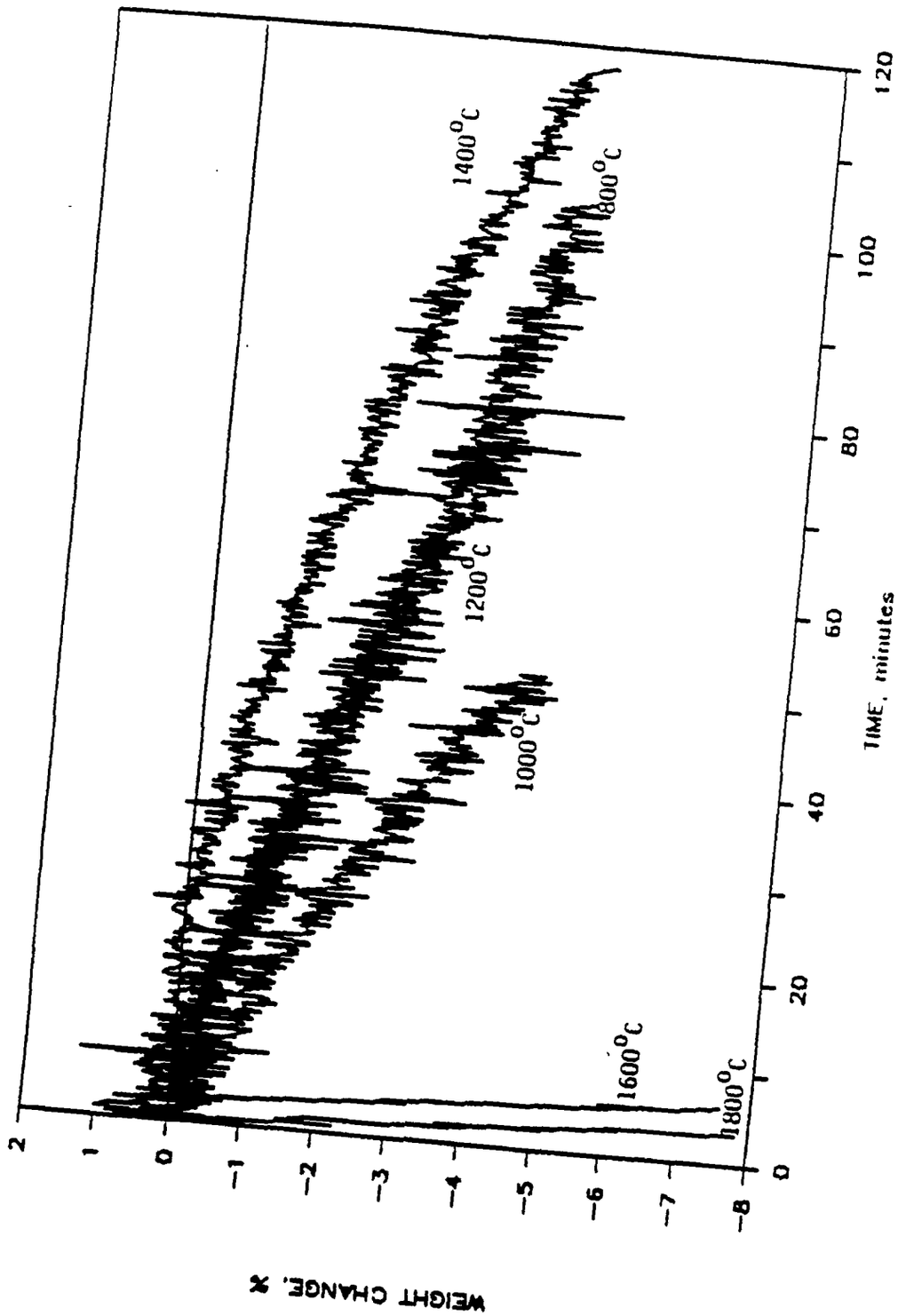

Figure 5. Oxidation Results at All Temperatures for the SiC + B_4C Coating Obtained with Al_2O_3.

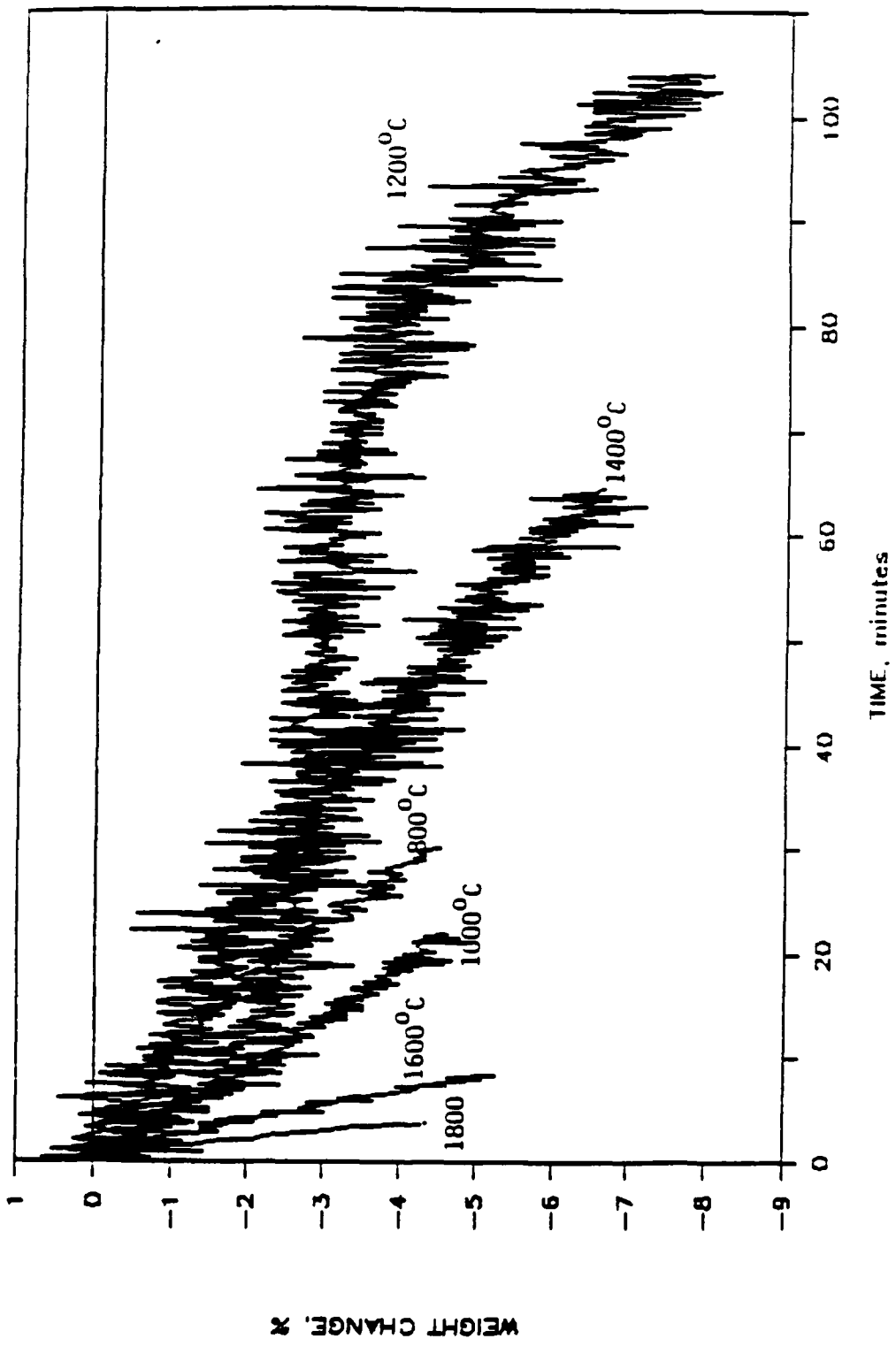

Figure 6. Oxidation Results at All Temperatures for the SiC Coating Obtained with Al_2O_3.

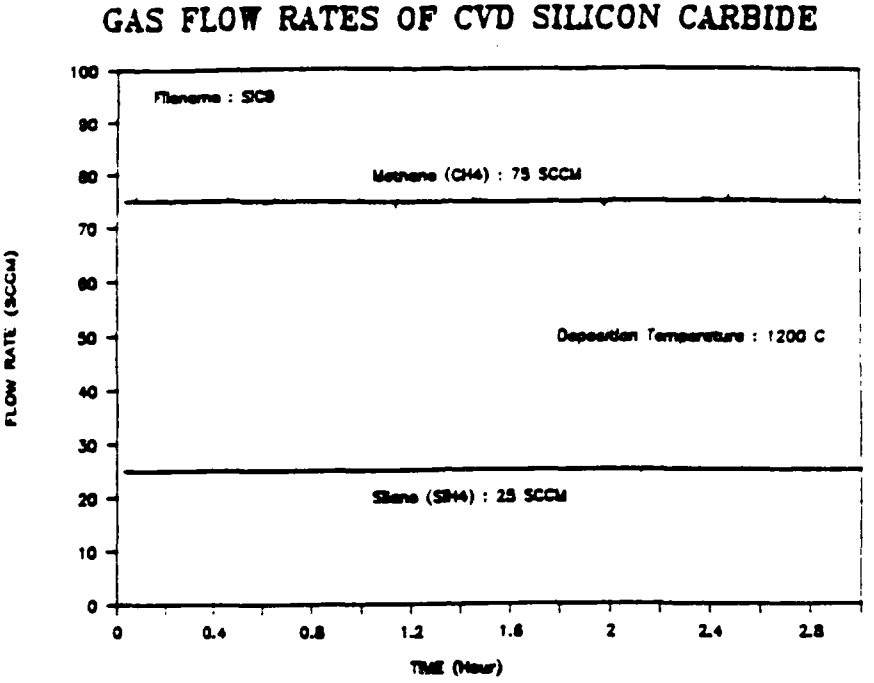

Figure 7. Experimental Flow Rate Curves for Obtaining a CVD SiC Coating.

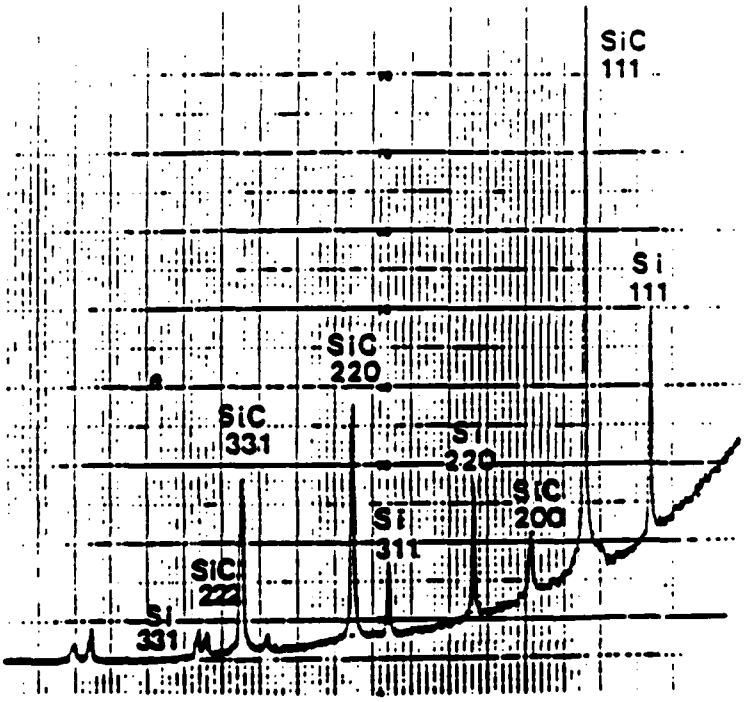

Figure 8. X-Ray Diffraction Spectrum of a CVD SiC Coated Composite.

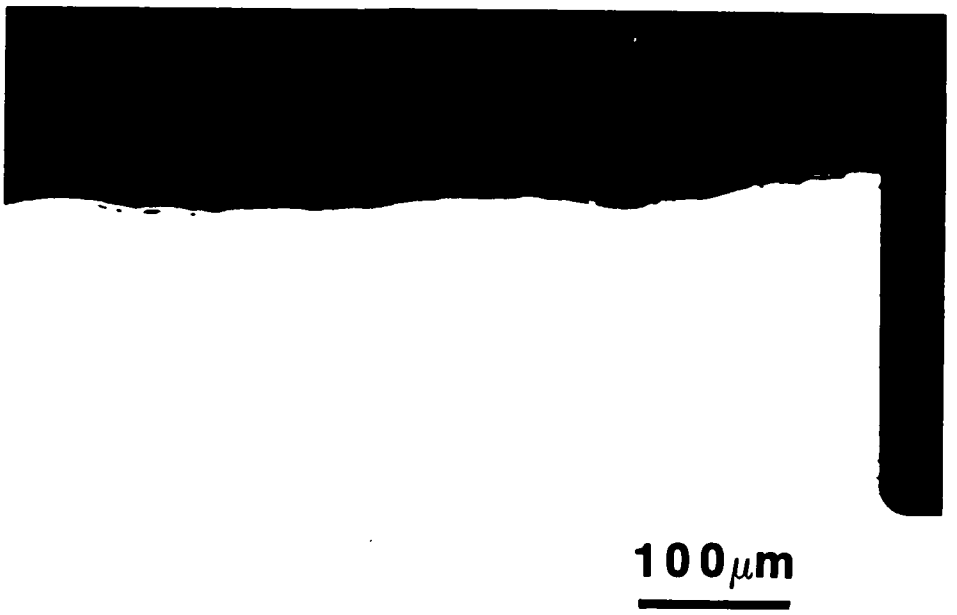

Figure 9. Cross-Section Optical Micrograph of a SiC-Coated Composite.

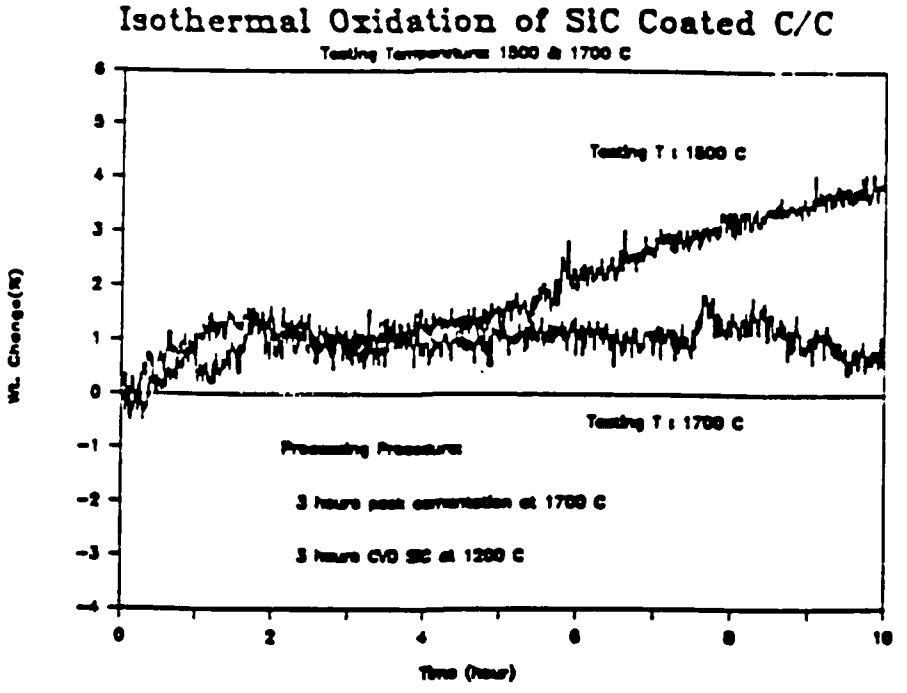

Figure 10. TGA Results of Two SiC Coated Specimens Oxidized at 1500°C and 1700°C isothermally.

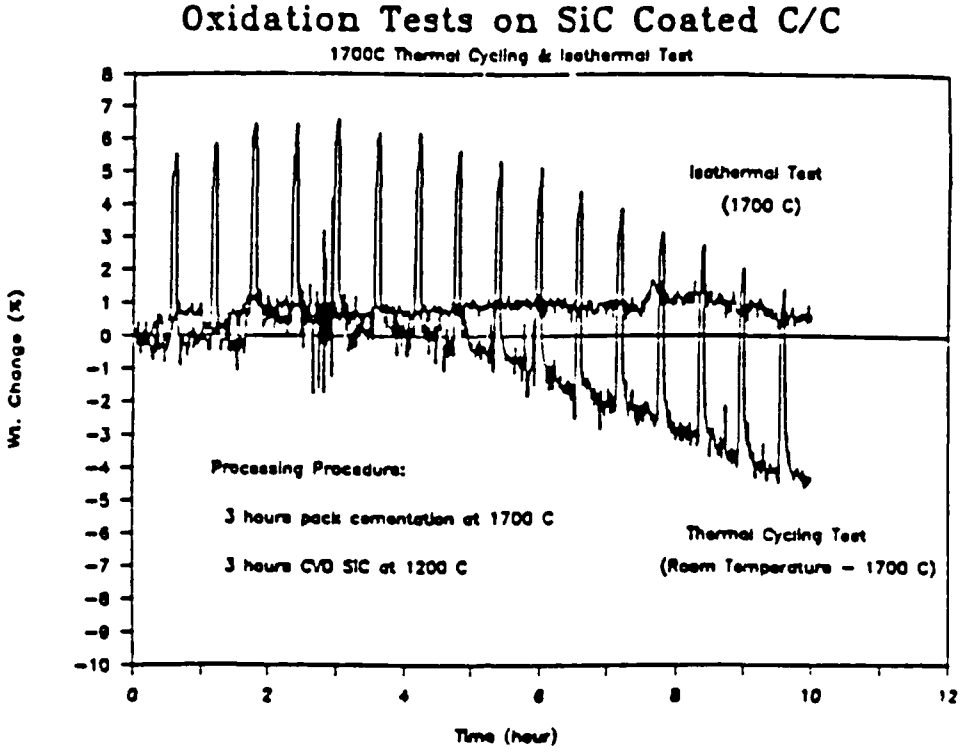

Figure 11. Comparison Between Isothermal and Thermal Cycling Tests at 1700°C for SiC-Coated Composites.

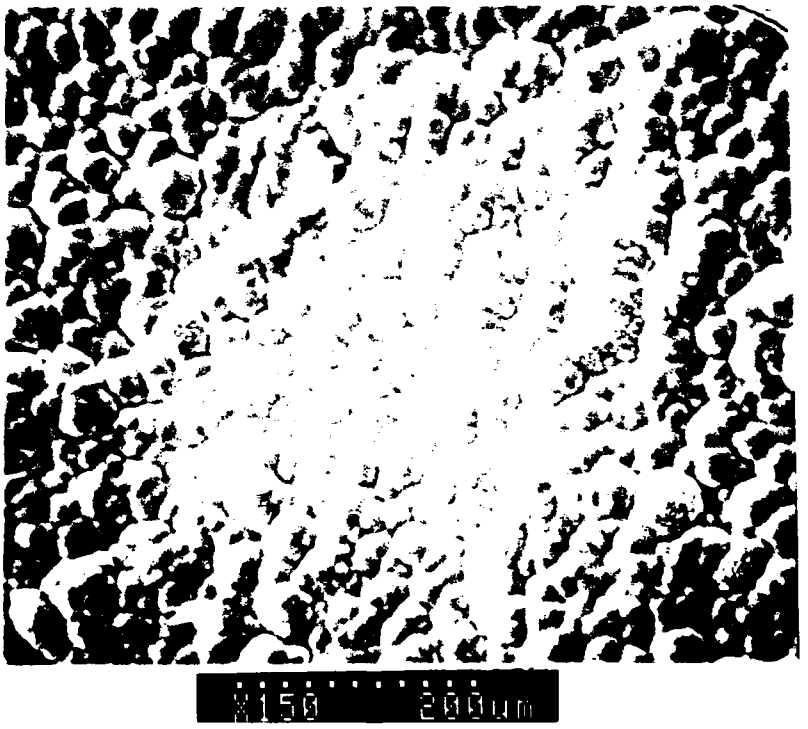

Figure 12. SEM Micrograph of a SiC-Coated Composite After a Oxidation Test at 1500°C, 10 Hours.

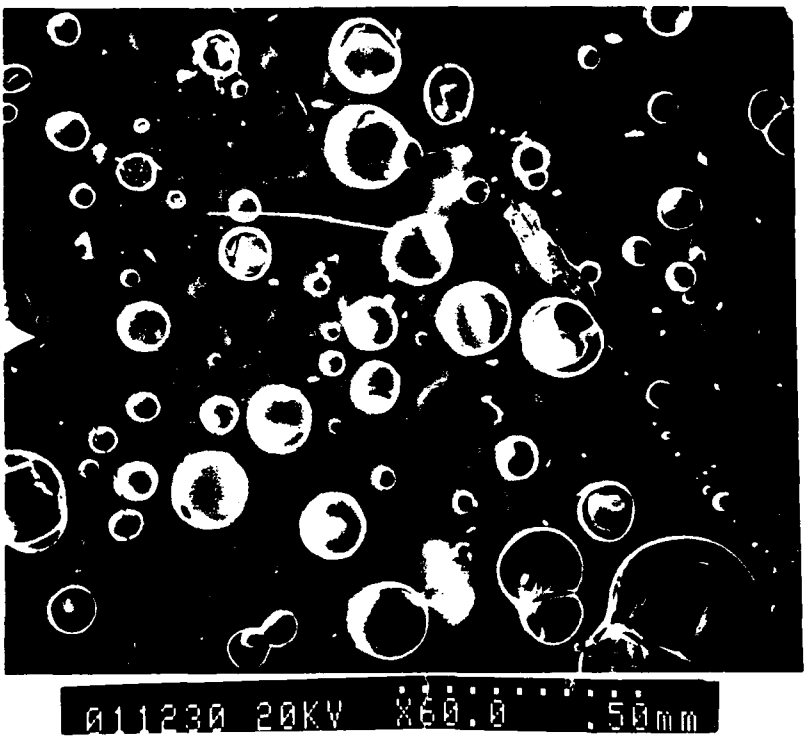

Figure 13. SEM Micrograph of an Oxidized SiC Coating. The Oxidation Test Was Performed at 1700°C for 3 Hours.

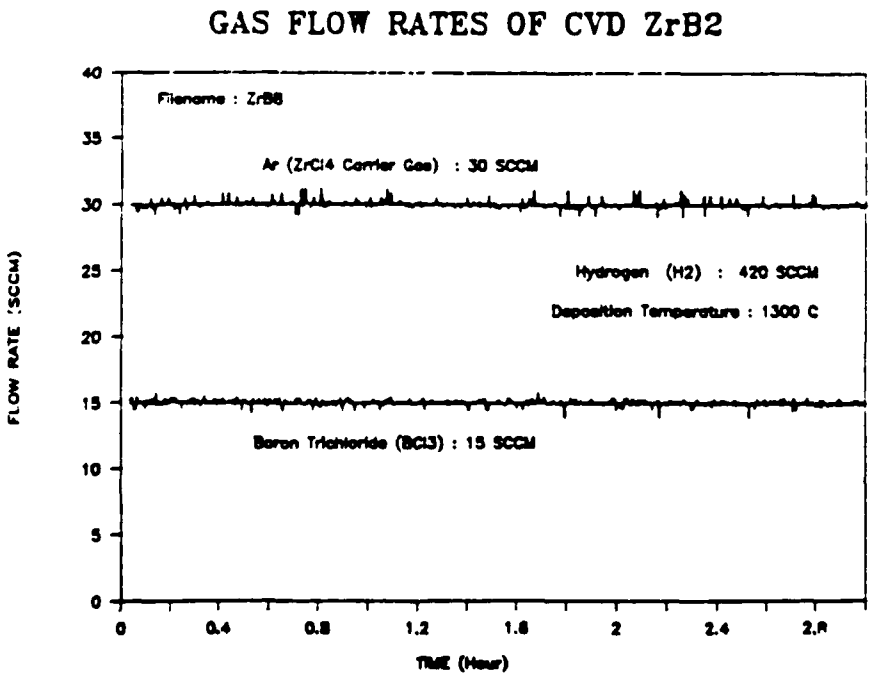

Figure 14. Experimental Flow Rate Curves for Obtaining a ZrB_2 Coating.

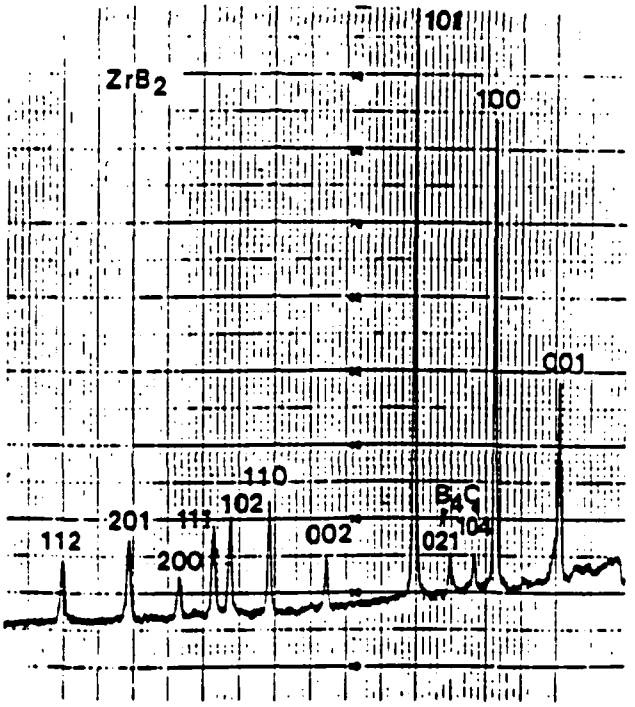

Figure 15. X-Ray Diffraction Spectrum of a ZrB_2 Coating. A Small Amount of B_4C Was Also Detected.

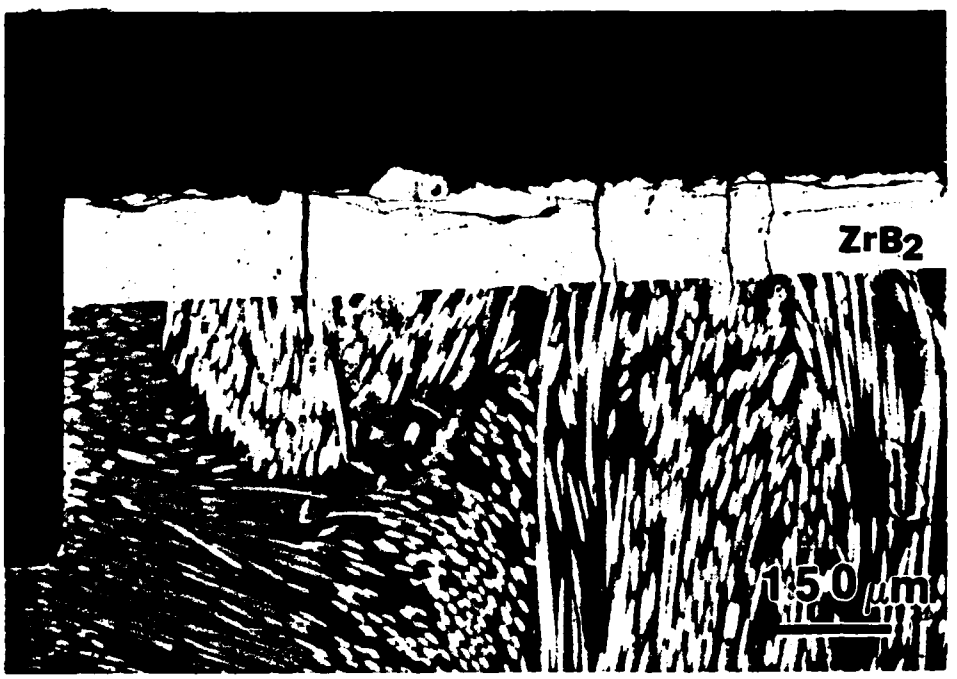

Figure 16. Cross-Section Optical Micrograph of a ZrB_2 Coating. The Coating Seemed to be Prone to Thermal Cracking.

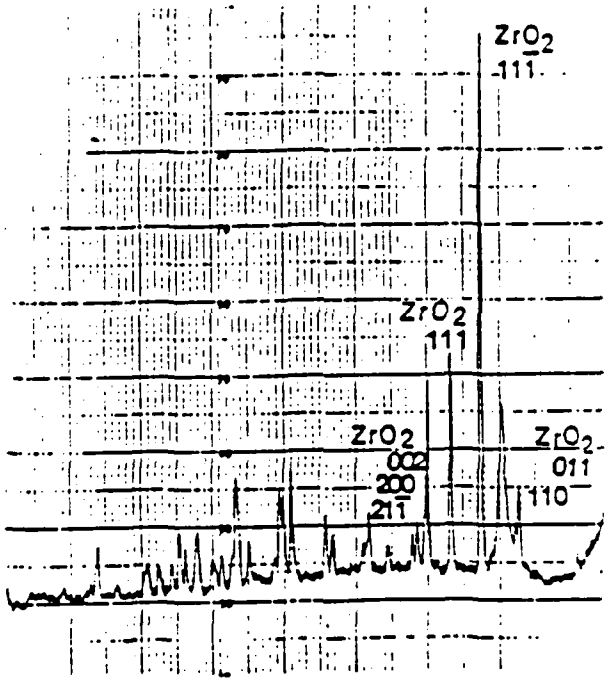

Figure 17. X-Ray Diffraction Spectrum of a Oxidized ZrB_2 Coating. After the Oxidation, the Residue Was Predominately ZrO_2.

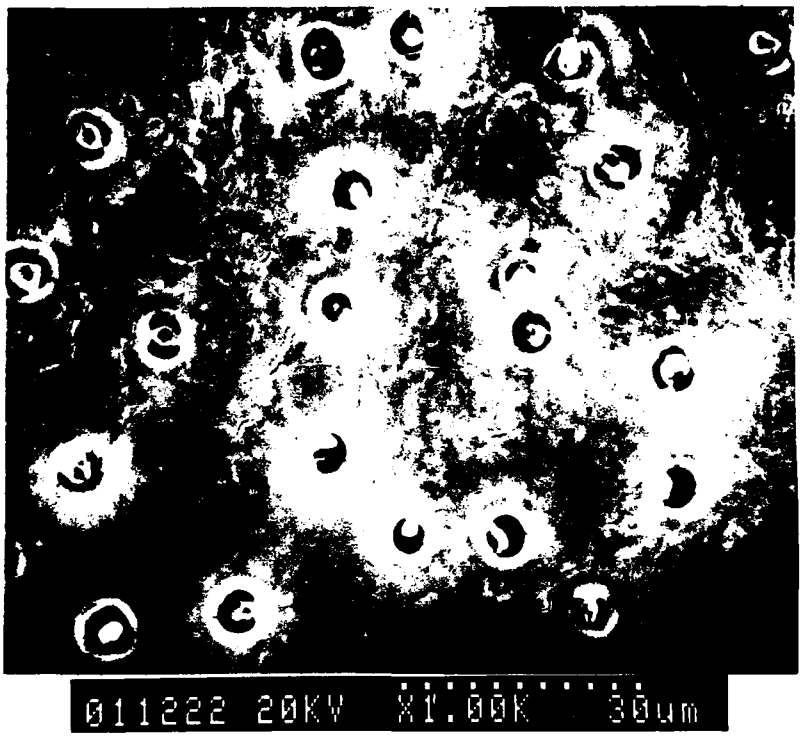

Figure 18. SEM Micrograph of a Oxidized ZrB_2 Coating. Rupturing of B_2O_3 Bubbles Started to Occur at about 1000°C, Leaving Particulate Residue of ZrO_2 Behind.

Figure 19. SEM Micrograph of a Badly Oxidized ZrB_2 Coating. The Laminar-Shaped Residue Was Proved by X-Ray Diffraction to be ZrO_2. The Coating Only Lasted a Few Minutes at 1500°C.

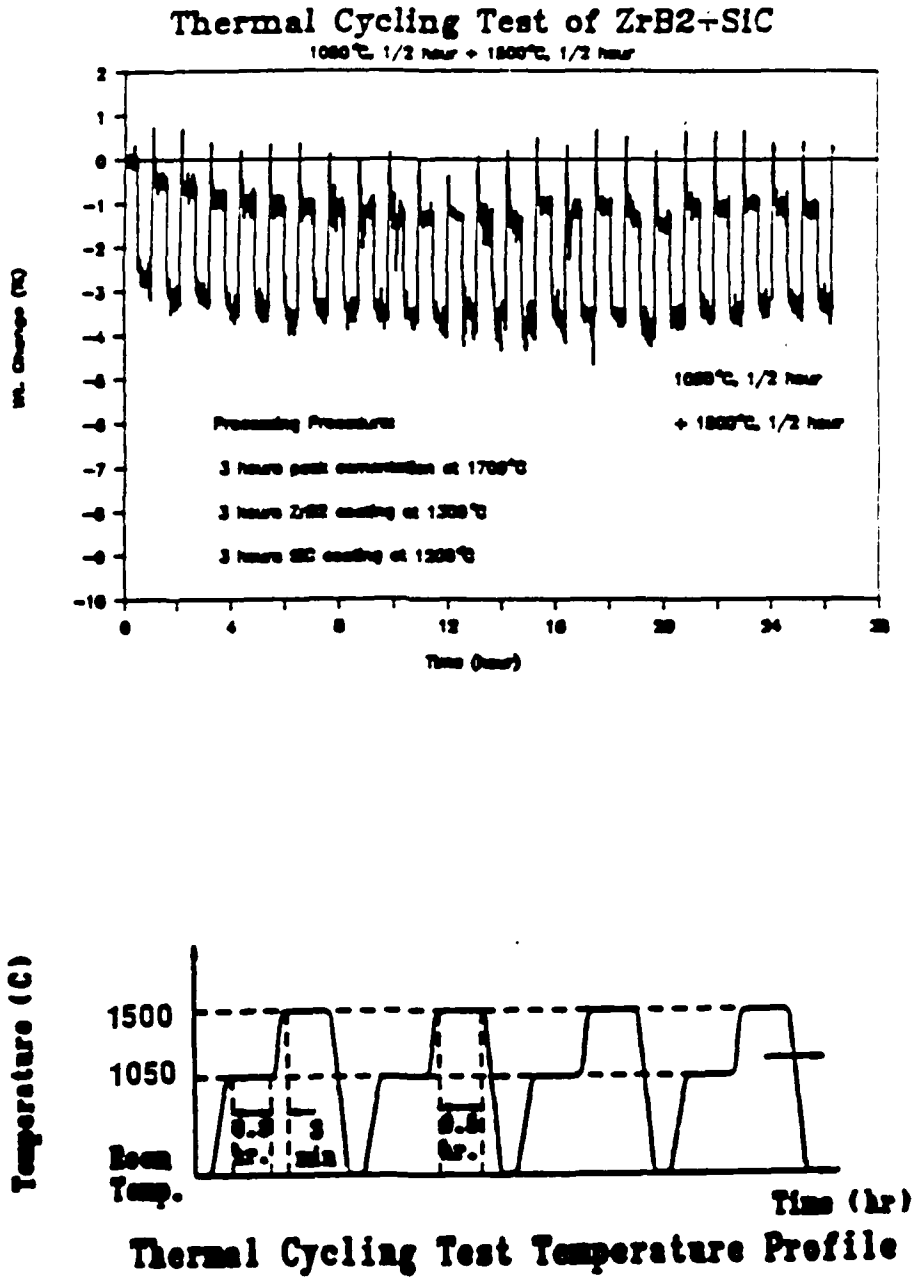

Figure 20. TGA Result of a Two-Stage Thermal Cycling Test Performed on a ZrB_2 + SiC Multilayer Coating. After 25 Hours of Cycling, the Specimen Lost Only 1% of Its Initial Weight.

Figure 21. SEM Micrograph of a ZrB_2 + SiC Multilayer Coating. Note that a Excellent Sealing Was Achieved in 3 Chipped Areas. The TGA Result of this Specimen is Shown in Figure 20.

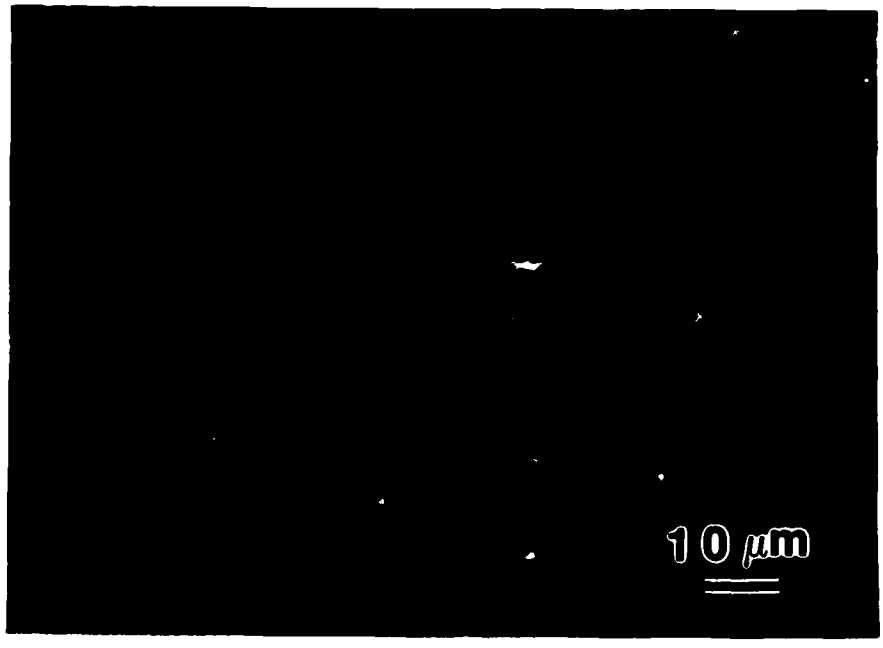

Figure 22. Optical Micrograph of the Cross Section of a Graded Coating Consisting of ZrC Layer (light region) and SiC (dark phase).

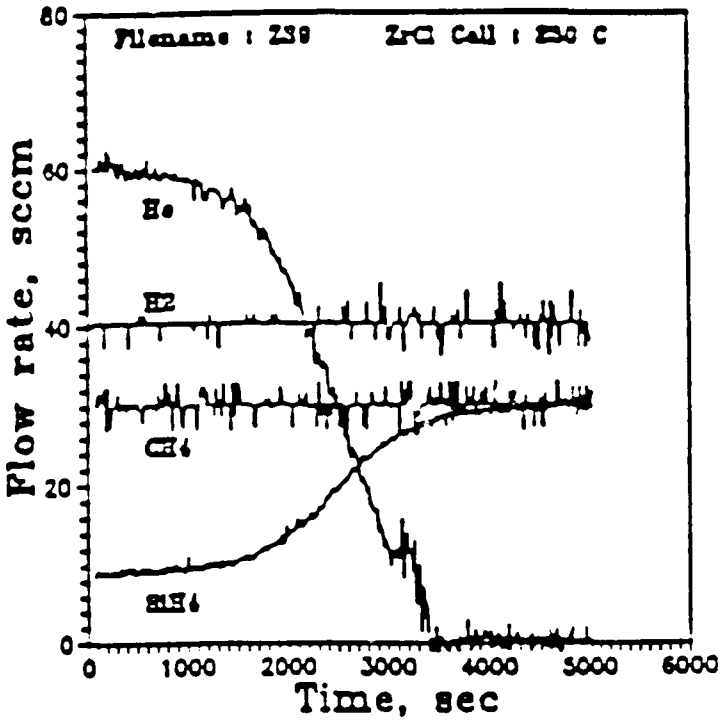

Figure 23. A Diagram Showing Flow Rate Curves as a Function of the Deposition Time for the Graded Coating Shown in Figure 22.

Figure 24. SEM Micrograph of an Oxidized Specimen Coated Using The Flow Condition Shown in Figure 23. This Specimen Was Oxidized at 1500°C for 10 Hours.

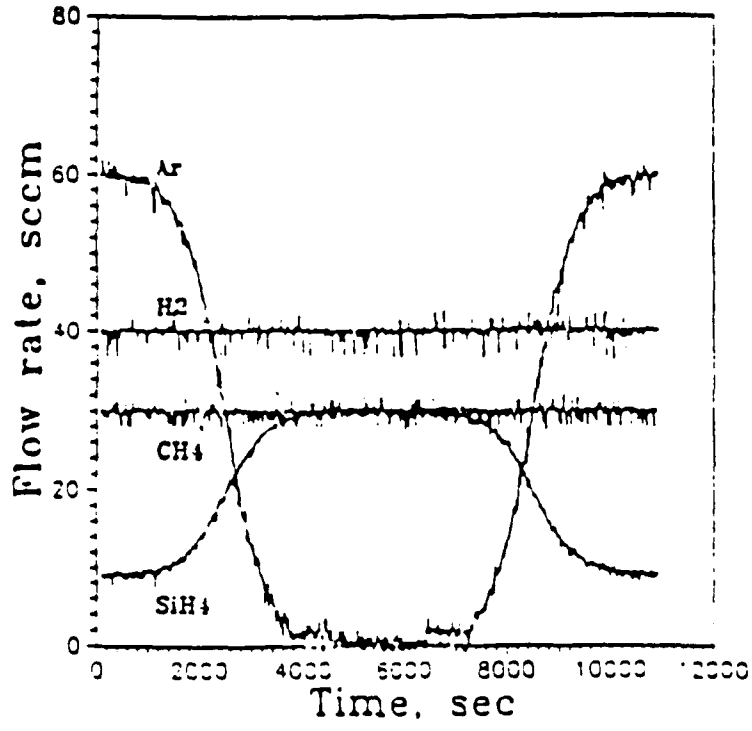

Figure 25. Flow Rate Curves for Obtaining the Optimum ZrC + SiC Graded Coating.

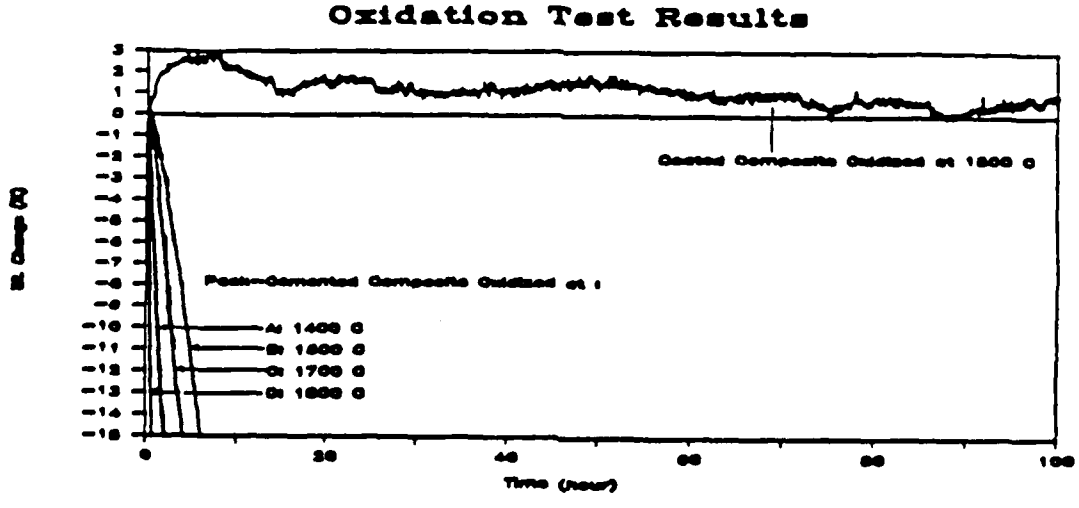

Figure 26. TGA Result of a Composite Protected by a Graded SiC + ZrC Coating at 1500°C in air, as Compared with the Test Results of Pack-Cemented Composites.

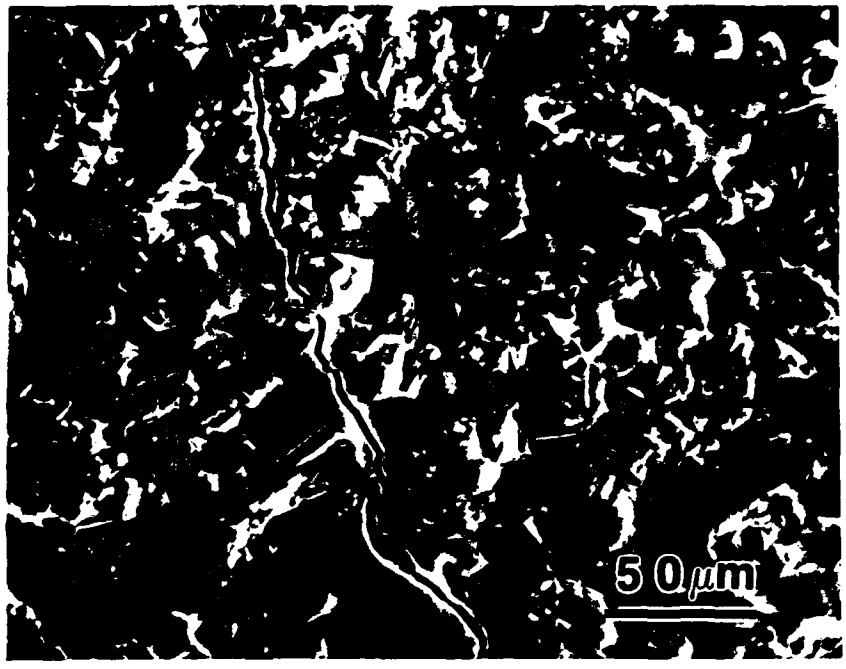

Figure 27. SEM Micrograph of a Coated Composite Oxidized at 1700°C, 10 Hours in Air.

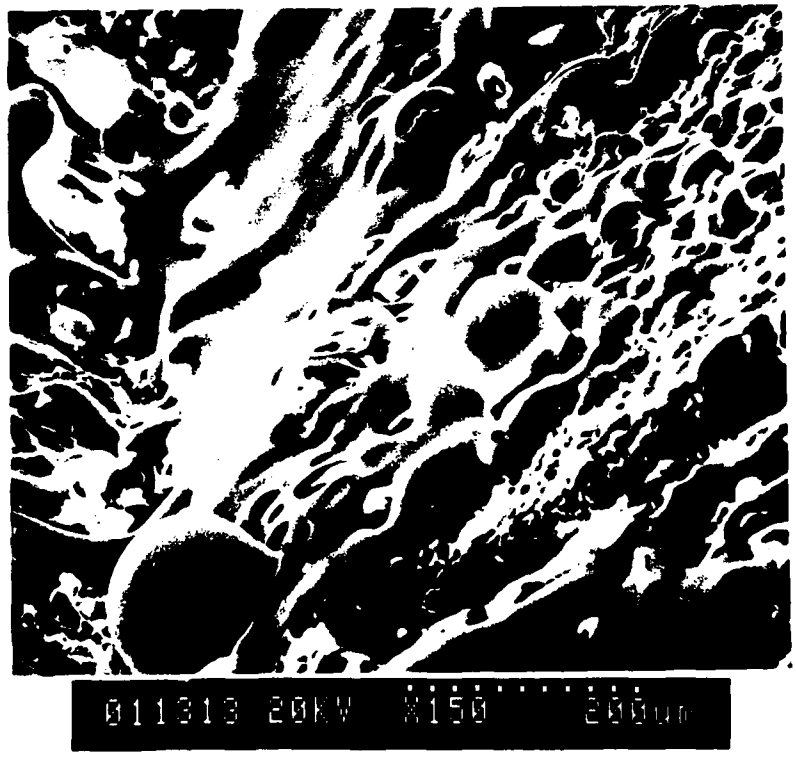

Figure 28. SEM Micrograph of the Surface of an Oxidized Specimen (1700°C, 21 Hours). Bubbles Were Formed During the Oxidation.

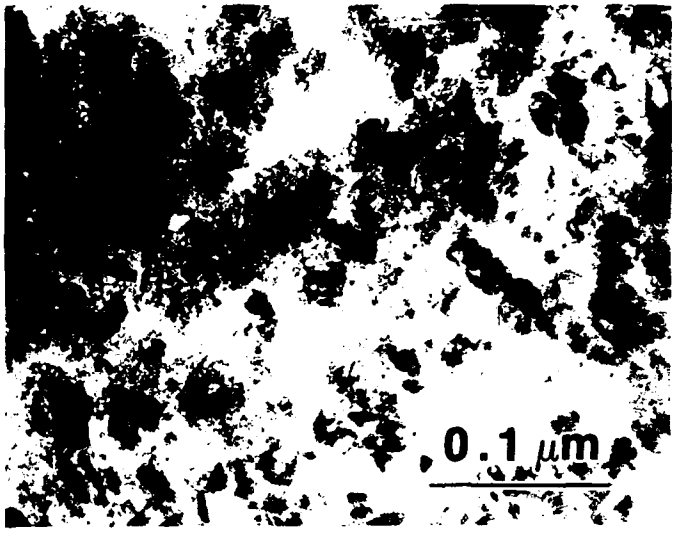

Figure 29. TEM Micrograph of a Glass Layer Formed on an Oxidized Specimen at 1700°C, 10 Hours in Air.

Figure 30. TEM Selecting Area (SAD) Pattern of the Glass Phase Shown in Figure 29.

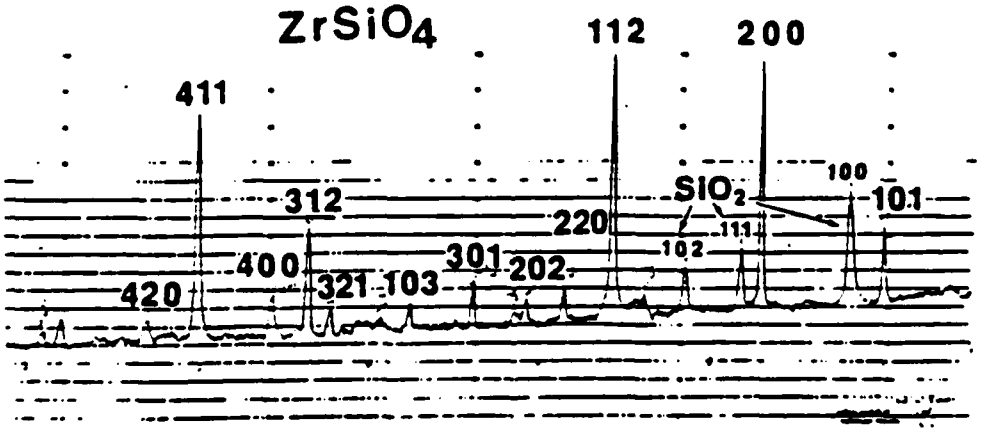

Figure 31. X-Ray Diffraction Spectrum of a ZrC + SiC Graded Coating Obtained Using the Flow Condition Shown in Figure 25. The Oxidized Surface Was Identified as $ZrSiO_4$ with a little amount of SiO_2.

ISOTHERMAL AND CYCLED OXIDATION RESISTANCE OF CERAMIC COATED CARBON-CARBON COMPOSITES

Jarlen Don*, Pawel Tlomak**, J. He*
*Department of Mechanical Engineering and Energy Processes
**Materials Technology Center
Southern Illinois University at Carbondale
Carbondale, IL

1. ABSTRACT

Isothermal and cycled oxidation behavior of coated carbon-carbon (C-C) composites is studied. Silicon carbide and zirconium diboride ceramic coating are deposited on pack cemented C-C substrates using a computer-controlled CVD system. Oxidation tests are performed using a thermogravimetric technique at temperatures up to 1700°C in air. Microstructure of the oxidized specimens is studied via optical and scanning electron microscopy. The oxidation data indicate that the effectiveness of the protective coatings is sensitive to both coating and oxidation testing conditions.

2. INTRODUCTION

With characteristics such as light weight, high heat of ablation, good thermal shock resistance, and good strength and toughness at high temperatures, carbon-carbon composites offer high performance in extreme thermal and chemical environments [1]. Potential uses have not only been identified in military aircraft, advanced missile systems, various hypersonic aerospace vehicles, but also as a very promising replacement for asbestos in brake lining and disc materials. Carbon-carbon composites are also applied in many other areas such as medical prostheses, and chemical plant heat exchangers. Although having excellent high temperature physical, mechanical, thermal and chemical properties, carbon-carbon materials experience severe oxidation in oxidizing environments and can last only over a very limited period of time at elevated temperatures [2]. The development of oxidation protection for carbon has been the subject of research for more than 50 years. The first effort directed towards carbon-carbon composite oxidation protection was conducted in the early 1970's on components to be used on shuttle orbiter vehicles. Since then, many types of protection techniques and systems have been developed for carbon materials, for high and ultrahigh temperature applications [3].

A successful oxidation-protection system should exhibit good mechanical and chemical stability under extreme thermal and oxidative environments. It should meet four main requirements: adequate adhesion between substrate and coating; maximum resistance to thermal shock and thermal cycling; good oxidation protection at both intermediate (1000°C) and high (>1500°C) temperatures; and good substrate oxidation resistance at moderate temperatures.

In this investigation, carbon-carbon composites were initially heat treated in Si-baring environments so that near-surface layers were converted to silicon carbide and then coated with SiC using chemical vapor deposition technique (CVD). Coated specimens underwent oxidation tests under isothermal and thermal cycling conditions followed by microstructural analysis using optical and scanning electron microscope, and X-ray diffraction.

3. EXPERIMENTAL PROCEDURE

3.1 Coating Deposition

Protective ceramic coatings were deposited using computer-controlled CVD system described elsewhere [4]. A commercial 2-D pitch/resin/CVI C-C composite have been chosen as a substrate. Each specimen was cut to dimensions of 0.5" x 3/8" x 1/4". Table 1 summarizes the source gases used and deposition conditions. Pack Cementation conditions used in this work were as previously reported [5].

Table 1. CVI deposition conditions.

Coating	Source gas	Temp	Pressure	Gas ratio
SiC	SiH_4, CH_4, H_2	1200°C	2 torr	SiH_4/CH_4 = 1/3
ZrB_2	$ZrCl_4$, BCl_3, H_2, Ar*	1300°C	10 torr	Ar/BCl_3 = 2/1

(*) Ar was used as a carrier gas for $ZrCl_4$ vapor.
ZrB_2 + SiC multilayer coating was deposited using the same conditions

The optimum CVD temperature for deposition of SiC coating was found to be about 1200°C. At this temperature, a smooth, SiC coating layer was deposited at a pressure of 2 torr and a SiH_4/CH_4 flow ratio of 1:3. The source gases used for the ZrB_2 coating experiments were $ZrCl_4$, BCl_3 and H_2. Similar to the ZrC coating experiments [4], Ar was used to carry the $ZrCl_4$ vapor into the reaction chamber. It was found that an Ar/BCl_3 ratio of 2:1 produces a pure ZrB_2 coating. An excess of H_2 was needed to reduce BCl_3. A series of test runs showed that a ZrB_2 coating could be deposited using 30 sccm of Ar, 15 sccm of BCl_3, and 420 sccm of H_2 at 1300°C and 10 torr of pressure.

3.2 Oxidation Tests

Two types of oxidation testings were employed in this study: isothermal tests and thermal cycling tests. Both types of tests were performed in air at atmospheric pressure using the homemade TGA apparatus consisting of an induction coil and a force transducer. The force transducer (vertek) measures the specimen weight and converts it linearly to an analog signal ranging from 0 to 5 volts. The analog signal is then recorded by an IBM personal computer through a data acquisition interface.

The specimens for oxidation tests were cleaned in methanol and dried in a vacuum desiccator for half an hour. The initial weight of each sample was measured using an analytical balance before the oxidation tests were carried

out. The specimen was placed in an alumina crucible, which was cut open near the bottom to provide access for air. The crucible was carefully hung inside the induction coil using a thin tungsten wire which was connected to the force transducer. During the test, an optical pyrometer was used to monitor the specimen temperature closely. The weight change was recorded by the computer and displayed on the monitor continuously throughout the test.

3.3 Microstructure Evaluation

In this study, microstructural characterization of coated and oxidized composites was conducted by using an optical microscope (ORM), the scanning electron microscope (SEM), and X-ray diffraction (XRD).

Specimens for optical microscopy were cut using a Buehler Isomet low speed saw to about 5mm x 12mm x 6mm size with a diamond wafering blade. Cut sections were then mounted in epoxy. Mounted samples were polished by using a Mini-Met polisher (Buhler). Polishing was done progressively from 600 grid to 1μm diamond paste. A Nikon Microphot optical microscope was used.

Samples for SEM studies were cut and mounted on SEM stubs using a conductive carbon cement. A sputtering technique was used to apply a thin (about 300 Å) coating of platinum on the sample surface. SEM observations were conducted by using a Hitachi S-570 scanning microscope.

The X-ray diffractometer used in this study was equipped with a Cu-tube and a Ni filter. The tube was operated at 35 KV and 15 mA. The monochromatic wave length was 1.54178 A. During each X-ray diffraction experiment, the detector was scanned at an angular speed of 2 degrees per minute. The chart recorder used to record spectra was normally run at a speed of 2 cm per minute.

4. RESULTS AND DISCUSSION

4.1 SiC Coating

Figure 1 shows a TGA thermogram of isothermal oxidation tests carried out in air at 1500° and 1700°C. No weight loss was found in either one of the specimens after 10 hours. On the contrary, the specimen oxidized at 1500°C gained 3.5% of its initial weight while the specimen oxidized at 1700°C showed less than 1% weight gain. Figure 2 compares the results of the isothermal test and the thermal cycling test at 1700°C. In the thermal cycling test, the temperature was cycled between room temperature and 1700°C, with a residence time of 0.5 hour at 1700° and a 3-minute period between each cycle. The thermal cycling test showed no significant weight change in the initial 6 cycles. Then, the specimen started to loose weight. After 10 hours of the cycling test, the specimen showed about 4.4% weight loss. The weight loss during the thermal cycling test was a linear function of time which indicated that the oxidation was reaction-controlled.

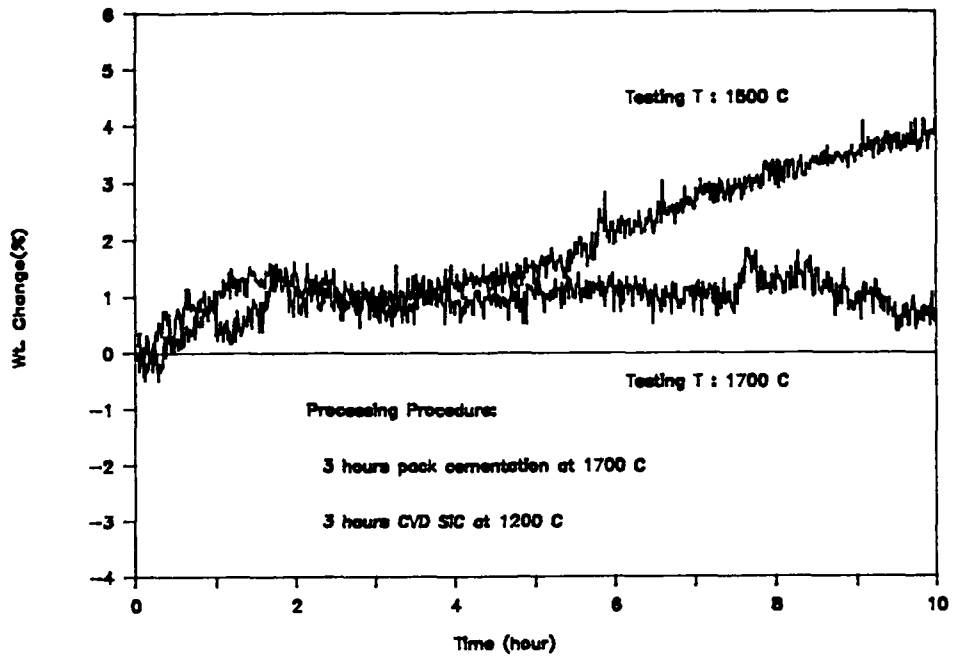

Figure 1. Isothermal Oxidation of SiC Coated C/C.

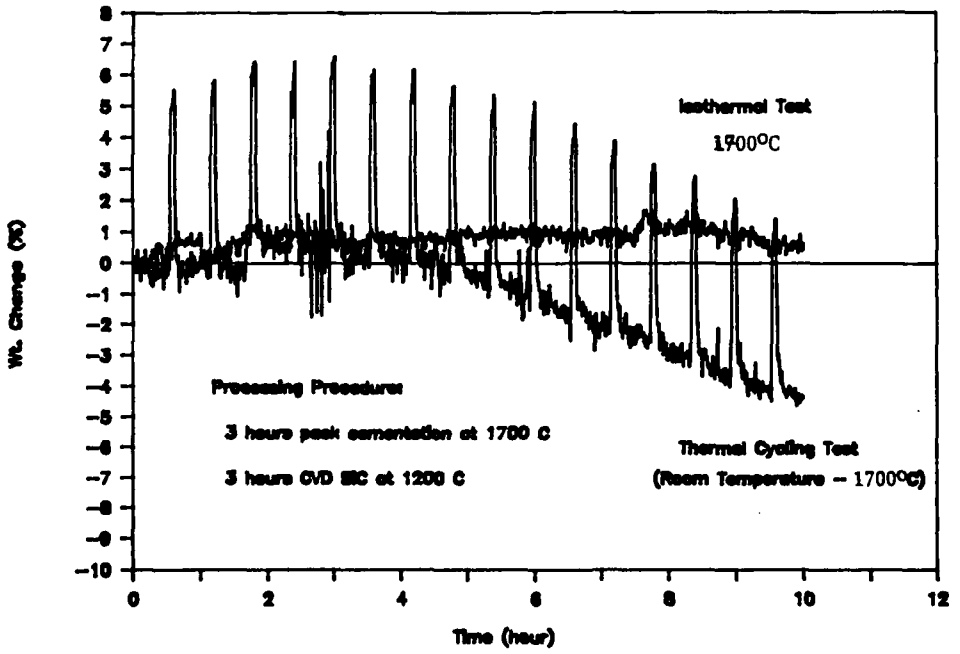

Figure 2. Oxidation Tests of SiC Coated C/C.

Figure 3 shows optical micrograph of the cross section of a SiC-coated composite after 3 hours of isothermal oxidation at 1700°C. A thin glass layer was found covering the entire surface of the specimen. A wavy, continuous, dark layer was found lying underneath the glass film. This dark layer is probably a carbon layer which is formed as a result of the interaction of the SiO_2 glass and the SiC coating:

$$SiC + O_2 ===> SiO_2 + C \qquad (3\text{-}1)$$

At the SiC/SiO_2 interface, the local activities of carbon and oxygen are not fixed, but rather, they depend upon the instantaneous thicknesses of the SiO_2 and the diffusivity in the SiO_2. Upon the arrival of oxygen by diffusion through the SiO_2, the interfacial oxygen should increase causing the activity of the carbon to rise. Since the temperature was high and the SiO_2 film was thin, the diffusion flux of oxygen may be high enough to cause carbon to become supersaturated. The supersaturated carbon then diffused downward and

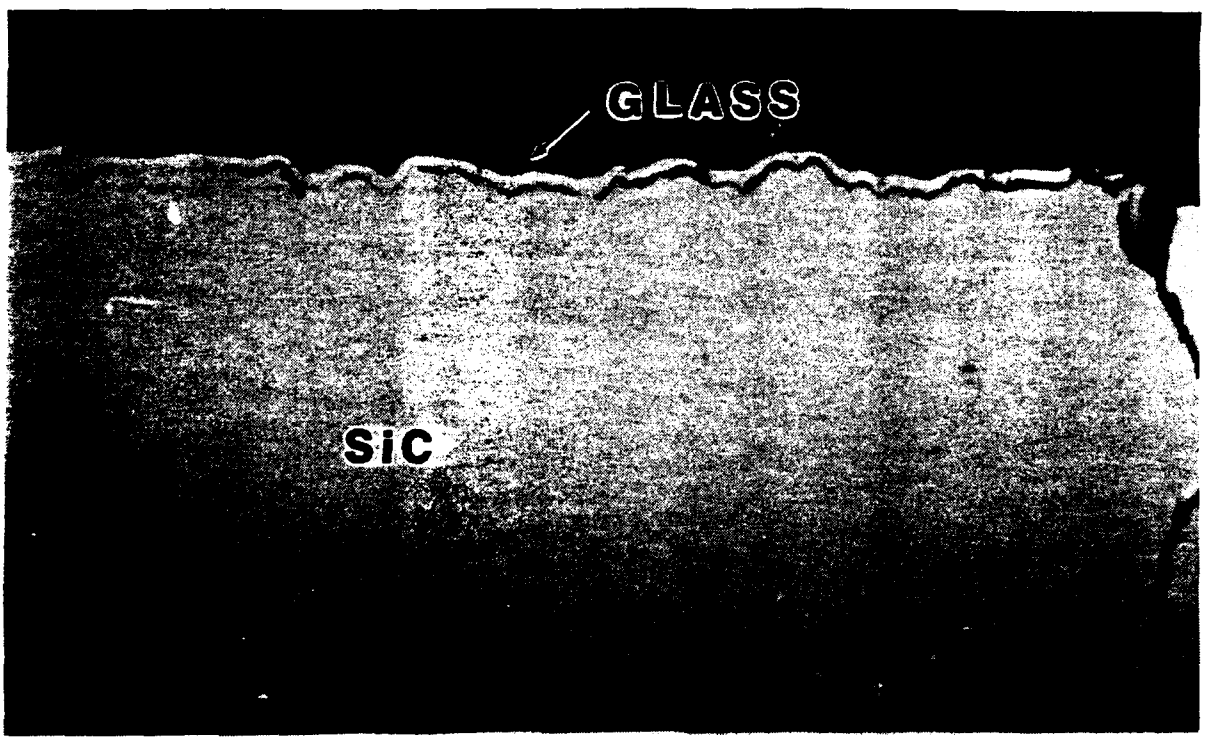

Figure 3. Cross-section optical micrograph of SiC-coated composite after isothermal oxidation test at 1700°C for 3 hours.

condensed into a subsurface carbon layer. Figure 4 is an SEM photograph of a SiC-coated specimen which was oxidized at 1500°C. No significant damage of the coating was found. However, oxidation at 1700°C causes bubble formation in a short period of time. Bubbling was observed after 3 hours of oxidation at 1700°C as shown in Figure 5.

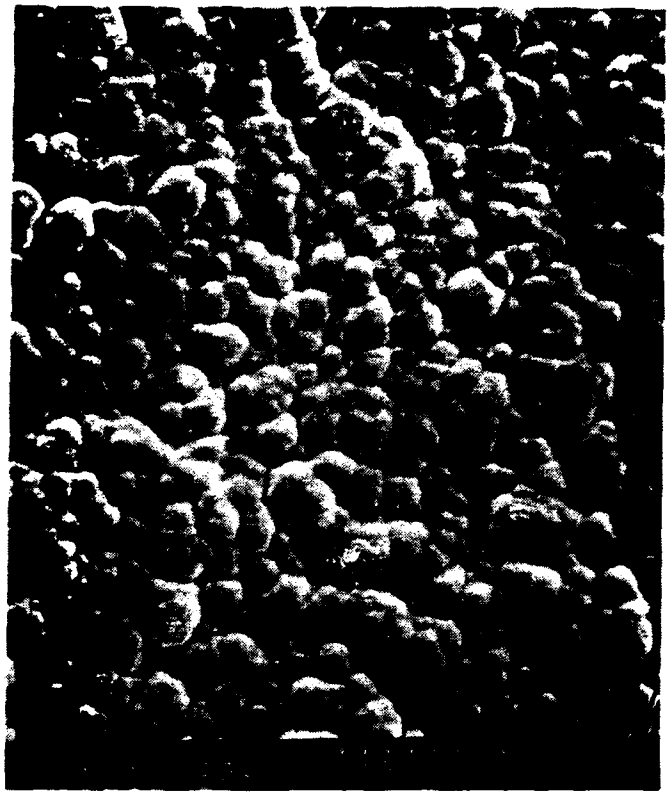

Figure 4. SEM micrograph of a SiC-coated composite after oxidation test at 1500°C, 10 hours.

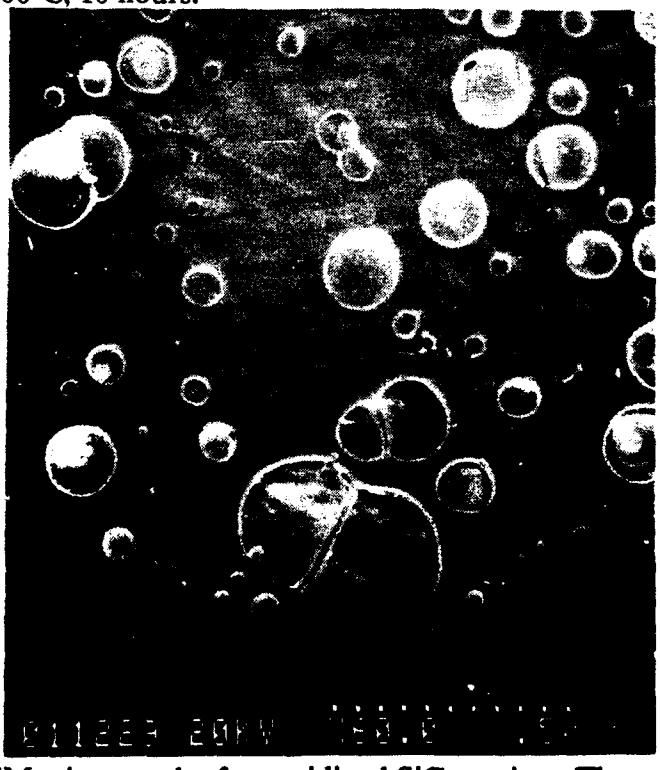

Figure 5. SEM micrograph of an oxidized SiC coating. The oxidation test was performed at 1700°C for 10 hours.

4.2. ZrB_2 Coating

An X-ray diffraction spectrum of a ZrB_2 coating is shown in Figure 6a. This pattern shows that the predominant phase in the coating is ZrB_2, along with a small amount of B_4C. The number of thermal cracks in this coating, however, was found to be higher than in the case of the SiC coating. This is because of the fact that the CTE of ZrB_2 (4.6×10^{-6}) is higher than that of SiC (3.6×10^{-6}) [7].

The oxidation results of ZrB_2 coating were not encouraging. The ZrB_2-coated specimen started to smoke extensively at about 1000°C and suffered severe weight loss when the temperature reached 1500°C. The oxidized specimen surface was partially covered with white powdery residue. X-ray diffraction performed on this residue showed that it was predominantly ZrO_2, as demonstrated in Figure 6b.

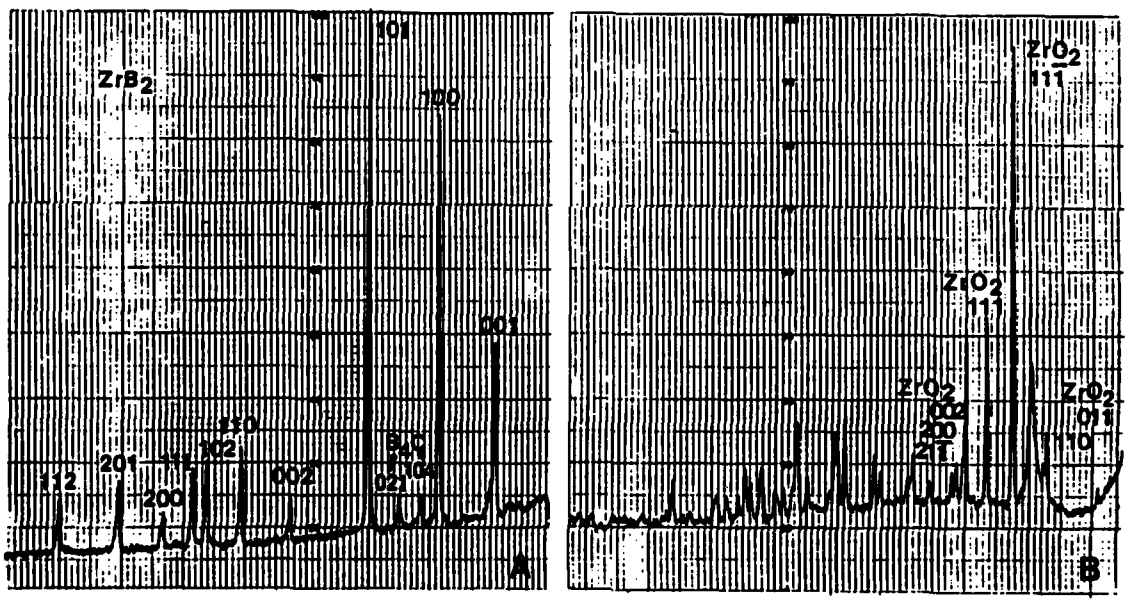

Figure 6. X-ray diffraction spectrum of ZrB_2 coating. A: Small amount ofB_4C was detected in the as-deposited coating; B:Oxidized coating showing predominantly ZrO_2.

In order to find out how and why ZrB_2 fails to protect carbon-carbon composite, an oxidation test was interrupted after 10 minutes and the specimen was examined by SEM. As shown in Figure 7, it was found that the glass sealant of B_2O_3 bubbled and ruptured easily, leaving particulate residue, presumably ZrO_2, where the bubbles ruptured. The remaining B_2O_3 glass, i.e., the background phase (Figure 7) also started to degrade. Microcracks began to develop due to the vaporization of B_2O_3 releasing the pressure of forming

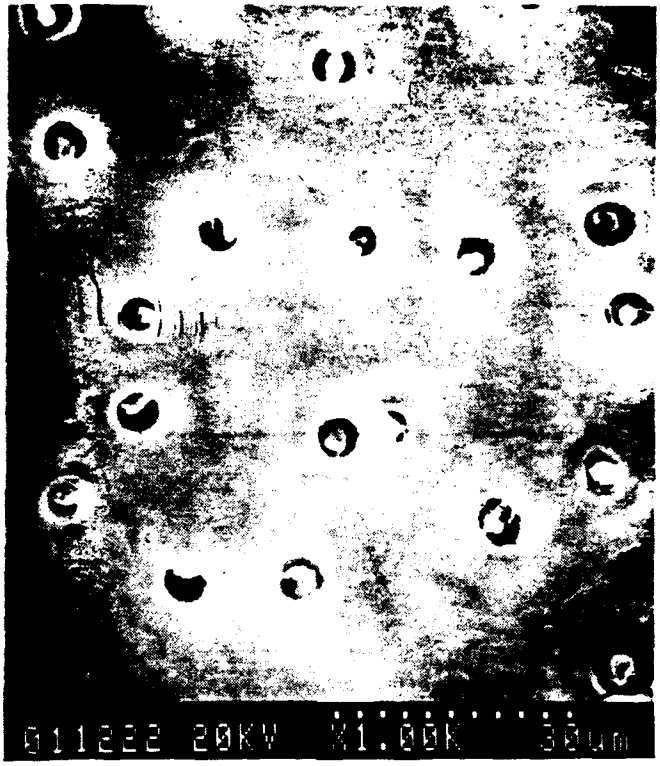

Figure 7. SEM micrograph of oxidized ZrB_2 coating. Rupturing of B_2O_3 bubbles started to occur at about 1000°C, leaving particulate residue of ZrO_2 behind.

Figure 8. SEM micrograph of an extensively oxidized ZrB_2 coating. The laminar-shpaed residue was identified using X-ray diffraction as ZrO_2. The coating last only a few minutes at 1500°C.

additional bubbles. Eventually, the layer of ZrO_2 was produced as shown in Figure 8. The events which occurred during the oxidation of the ZrB_2 coating indicated that Zr was not involved in forming a passive Zr-containing borate glass. The oxidation reaction of ZrB_2 seemed to be

$$ZrB_2 + 5/2\ O_2 = = = > ZrO_2\ B_2O_3. \qquad (3\text{-}2)$$

The B_2O_3 product vaporized quickly since it was the only low melting point compound (449°C [6,7]).

Although ZrB_2 was not qualified as an independent protective coating, it was interesting to note that this coating started to form B_2O_3 glass at a temperature lower than 1000°C. It may help to improve the protection of carbon-carbon composites at intermediate temperatures. Therefore, if ZrB_2 is used in conjunction with SiC coating, better thermal cycling properties should be expected. This leads to the approach of SiC + ZrB_2 multilayer coating.

4.3. SiC and ZrB_2 Multilayer Coating

The multilayer coating of SiC + ZrB_2 consisted of an inner layer of ZrB_2 and an overcoat of SiC, Figure 9. The SiC overcoat retards the vaporization of the borate glass. As described earlier, this composite coating is expected to offer good oxidation protection at both intermediate and high temperatures. Since efficient protection is expected to cover a wide temperature range in this

Figure 9. Optical micrograph of SiC + ZrB_2 multilayer coating.

multilayer approach, the thermal cycling test was of primary interest in the study of this approach. In particular, a new type of 2-stage thermal cycling test was designed which included residence time periods at both intermediate and high temperatures in a cycle. Figure 10 presents a TGA thermogram of a 2-stage thermal cycling test performed on a multilayer-coated composite. During the test, the temperature was cycled from room temperature to 1000°C for half an

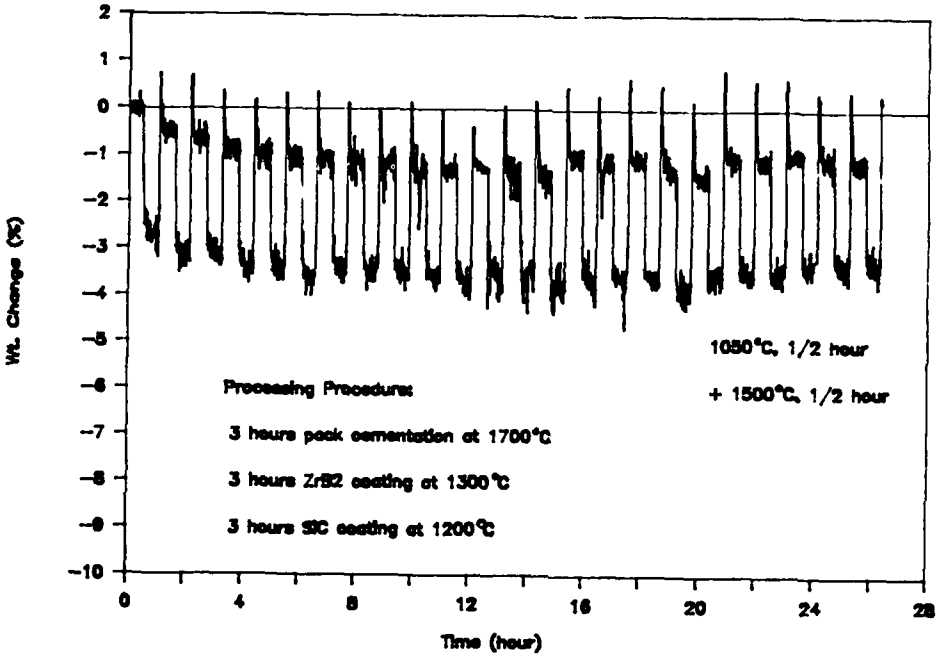

Figure 10. Thermal cycling test for ZrB_2 + SiC coating.

hour followed by 1500°C for another half hour. After 25 hours of testing, the specimen showed a uniform, reflective, glassy surface without any trace of oxidation damage. The total weight loss of the specimen was less than 1%. SEM observations showed that a few chipped areas caused by prior CVD cool down were all perfectly covered with glass, Figure 11. Apparently, glass flowed efficiently at 1000°C and remained stable at 1500°C. It indicated that B_2O_3 and SiO_2 reacted readily, leading to the formation of borosilicate glass which provided good protection over a wide temperature range. Additionally, no evidence of ZrO_2 was found. This implies that no Zr was contained in the glass, and it may have offered an advantageous effect to the glass.

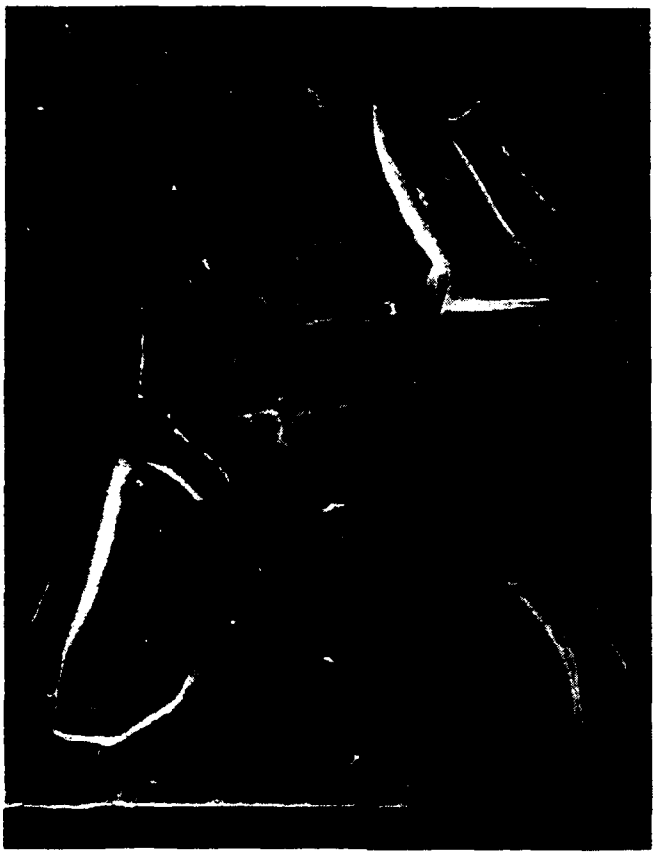

Figure 11. SEM micrograph of a ZrB_2 + SiC multilayer coating. Note that excellent sealing was achieved in 3 chipped areas.

5. CONCLUSIONS

1. Mixed SiC and Si coating shows improved oxidation protection over the pure SC coating.

2. ZrB_2 coating does not provide satisfactory oxidation resistance at temperatures below 1500°C. B_2O_3 glass formed during oxidation at these temperatures vaporizes and leaves a ZrO_2 layer on the surface of the coated C-C composite.

3. Coating consisting of ZrB_2 and SiC overlayer shows improved oxidation resistance at temperatures below 1500°C. The total weight loss of less than 1% was observed after 25 hours of 2-stage thermally cycled oxidation testing.

6. REFERENCES

1. Fitzer, E., (1987), "The Future of Carbon-Carbon Composites," Carbon, 25, 163-190.

2. McKee, D. W. (1986), "Oxidation Behavior and Protection of Carbon-Carbon Composites," Carbon, 25, 551-557.

3. Strife, J. R. and Sheehan, J. E. (1988). "Ceramic Coatings for Carbon-Carbon Composites," Am. Ceram. Soc. Bull., 67, No. 2, 369-374.

4. Don, J., Tlomak, P., He, J., and Stojak, J. (1989), "Ceramic Coatings for Oxidation Inhibition of C-C Composites," in Proceedings of the 13th Conference on Metal Matrix, Carbon, and Ceramic Matrix Composites, Cocoa Beach, Florida, January 18-21, 599-608.

5. Rogers, D. C., Shuford D. M., and Mueller, J. I. (1975). "Formation Mechanism of a Silicon Carbide Coating for a Reinforced Carbon-Carbon Composite," in Proceedings of the 7th National SAMPE Technical Conference, 319.

6. D. W. McKee, C. L. Spiro and E. J. Lamby, "The Effects of Boron Additives on the Oxidation Behavior of Carbons," Vol. 22, No. 6, pp. 507-511, 1984.

7. "Handbook of Chemistry and Physics," 54th edition, CRC Press, (1974).

ACKNOWLEDGMENTS

We wish to acknowledge the Air Force Office of Scientific Research for providing the funding for this research under contract AFOSR-88-0130.

Microstructure of Pack Cemented SiC Protective Coatings for Carbon-Carbon Composites

P. Tlomak, C.P. Ju, S. Takano, J. He*, J. Stojak*, and J. Don*
Materials Technology Center
and *Department of Mechanical Engineering and Energy Processes
Southern Illinois University at Carbondale,
Carbondale, IL

Abstract

This report documents the results of ongoing research on the microstructure of pack cemented carbon-carbon (C-C) composites. Optical and transmission electron microscopy are used for overall and detailed microstructural characterization. A microstructural comparison of the following systems is presented: pitch/resin/CVI, PAN/CVI, and PAN/pitch. The tendency for composites to convert to silicon carbide (SiC) is found to vary from one system to another, depending on the type, microstructure, and crystallinity of both the fiber and the matrix. The macroscopic and microscopic porosity induced during processing can enhance such tendency by providing open channels for silicon penetration. The carbon-SiC transformation occurs preferentially at microstructural imperfections such as micropores and microcracks and the various interfaces in the composites. The converted SiC crystals are essentially equiaxed and randomly oriented, regardless of their precursor orientation, i.e., the strong preferred orientations, exhibited in fibers, mesophase pitch, and CVI are completely destroyed after converting to SiC.

Introduction

Carbon-Carbon (C-C) composite materials are promising for a variety of high-temperature structural applications due to their unique thermal and mechanical properties [1]. In many uses C-C composites are required to perform in high-temperature oxidizing environments. Unfortunately, C-C composites are susceptible to oxidation and gasify rapidly in ambient air at temperatures as low as 500° via the formation of CO and CO_2 [2]. Consequently, the development of oxidation protection systems for structural C-C composites has received worldwide attention.[3,4] Current attempts to provide oxidation protection for C-C composites include both incorporating oxidation inhibitors into the composite during fabrication and applying an external ceramic protective coating.

C-C composites are usually fabricated by carbonization of resin or pitch precursors which have infiltrated in liquidous form into a carbon fiber preform, or by chemical vapor infiltration (CVI) of pyrolytic carbon. In either case, generation of open and closed porosities and cracks is unavoidable [5]. Such porosities form by gas generation, matrix material shrinkage during carbonization, and during heating and cooling due to incompatible CTE's between fiber and matrix [6]. Consequently, several cycles of infiltration and the subsequent heat treatments are commonly used in attempts to obtain a higher density.

For the oxidation protection of C-C composites at temperatures below about 1650°C, silicon-based ceramic coatings such as SiC or Si_3N_4 are commonly used [7]. Upon exposure of such coatings to a high-temperature oxidizing atmosphere, a protective SiO_2 layer is formed providing an effective oxygen diffusion barrier for the underlying C-C substrate. A variety of deposition techniques, including plasma spray, CVD, and reaction bonding have been developed to provide good adherent SiC protective coatings. In addition to such deposition techniques, a pack cementation process has been developed and has already been applied for oxidation protection of Space Shuttle Leading Edges [8].

This protection system, which was composed of a SiC conversion layer and a silicate glaze overlay, had been proven to perform well under conditions of rapid heating and cooling.

The mechanism of C-C composite surface conversion to SiC during pack cementation includes two aspects. The first is a process in which molten silicon reacts with carbon to form SiC, and the second involves reaction between gaseous silicon-containing species and carbon [9]. The roles of composite microstructure, crystallinity, internal cracks and porosities, and fiber-matrix interface morphology in the conversion process, however, are little understood.

The present study investigates such effects on both macro- and microstructural levels. Commercial 2-D PAN/CVI, 2-D pitch/resin/CVI, and 3-D PAN/pitch systems are studied. This work is an integral part of the ongoing research on the oxidation protection performance of the various pack cemented C-C composites.

Experimental

Three types of C-C systems were selected for this study, i.e., pitch/resin/CVI, PAN/CVI, and PAN/pitch. Specimens for pack cementation were cut to dimensions of 0.5" x 3/8" x 1/8". The pack cementation process was similar to that used by Rogers et al. [9]. Specifically, each specimen was placed in a graphite crucible and entirely buried in a powder mixture composed of 10 wt% of Al_2O_3, 60 wt% of SiC, and 30 wt of% Si. After drying at 100°C for 16 hours in vacuum, the packed crucibles were fired at 1700°C for 3 hours in argon under ambient pressure, as shown in Figure 1. When completed, the specimens were removed from the crucibles and showed a grey-green color and a rough surface which revealed some surface features.

The overall morphological information such as the size, shape and distribution of converted regions as well as macrocracks and macropores in both unconverted and converted C-C composites was obtained using a Nikon Microphot optical microscope. The different interference reflections (in the polarized light mode) appearing on the polished sample surface are due to the differences in crystallite orientation [10]. Isotropic carbons exhibit a purple interference color, while anisotropic carbons appear yellow or blue (depending on relative orientation of basal planes with respect to the direction of the light). Image analysis (Image Technology Corporation) was used to measure the relative amount of porosity and the average thickness of SiC conversion layers.

Detailed microstructure of converted C-C composites was characterized using transmission electron microscopy (TEM) technique. Interfacial regions between fibers and matrix and between unconverted and converted portions, as well as internal cracks and porosities were examined. The size, shape and orientation of graphitic crystallites and turbostratic regions both adjacent to and away from interfaces were determined using bright field (BF), dark field (DF), and selected-area diffraction (SAD).

Preparation of the carbon-carbon thin foils for TEM involved mechanical dimpling followed by argon atom milling. Specimens about 500 microns thick were sliced from bulk composite using a diamond saw. Three millimeter diameter discs were then cut from each slice using a drilling press. These discs were mechanically dimpled (VCR Group D500 mechanical dimpler), from the substrate side, to a thickness of roughly 10 μm (a 0.5 μm diamond paste was used for the final stage). The dimpled discs were then atom milled (ION TECH FAB 306 atom miller) until perforation.

Results

Optical Microscopy

Optical microscopy was performed to obtain the overall morphological information on the pack cemented SiC layers, such as their thickness and distribution. The temperature profile of pack cementation process is shown in Figure 1, and the conversion layer thickness data is given in Table 1. Among the two 2-D C-C composites investigated in this work, the thinner SiC conversion layer, i.e. a layer approximately 180 microns thick, is formed on the surface of the 2-D PAN/CVI composite, as compared with approximately 320 microns thick SiC conversion layer of the 2-D pitch/resin/CVI composite (table 1). These SiC conversion layers are uniformly distributed across both sides of these composites which are parallel to the fiber weave direction. Unlike them, SiC conversion layers formed on sides which are perpendicular to the fiber weave direction are nonuniform and their thicknesses vary depending on fiber weave geometry and local porosity distribution. The thickest SiC conversion layer, approximately 430 microns thick is formed on the surface of the 3-D PAN/pitch composite in the fiber bundle area. Matrix pockets of this composite are almost fully converted.

The polarized light micrographs (Figure 2) represent the microstructure of a transverse fiber bundle of as-fabricated (Figure 2a) and converted (Figure 2b) 2-D pitch/resin/CVI C-C composites. As seen in Figure 2a, the two pitch fiber bundles of the unconverted composite are bonded by an interbundle resin char. Some internal pores and cracks exist in both interbundle and intrabundle regions. Different interference contrast colors (not shown in the black-and-white micrographs in this paper) indicated that resin and the transverse sections of fibers are isotropic, whereas the CVI layers are anisotropic. Figure 2b shows an extensively transverse fiber bundle containing an open crack. It can be seen that silicon reacts preferentially with the carbon surrounding the open crack which provides a channel for silicon penetration to the composite interior (from left to right in Figure 2b). The first CVI layer (the layer next to fiber surface) appears to be more resistant to conversion than the second (the outer) layer of CVI carbon as indicated in Figure 2b.

Optical micrographs of polished sections of the converted and unconverted 2-D PAN/CVI C-C composite are shown in Figure 3. This composite consists of a large amount of porosities. Fibers lying outside of the bundle are covered with a much thicker layer (thicker than fiber diameter) of CVI carbon. During pack cementation, only outer portion of CVI carbon was converted, Figure 3b. The preferential conversion "outlining" the porosities seen in Figure 3b indicates that these porosities were open to the environment during pack cementation.

Figure 4 shows optical microstructure of the converted and unconverted 3-D PAN/pitch C-C composite made of orthogonal arrays of continuous fiber bundles in pitch matrix. The longitudinal and transverse fiber bundles, interbundle matrix pockets, as well as interbundle and intrabundle cracks and pores are shown in Figure 4a. During pack cementation a large portion of interbundle matrix material in this area was converted to SiC, especially in the vicinities of pores, Figure 4b. The interbundle and intrabundle cracks enhanced conversion of both pitch matrix and PAN fibers as shown in Figures 4c and 4d.

Transmission Electron Microscopy

TEM microstructure of a transverse section of the pack cemented 2-D pitch/resin/CVI C-C composite is shown in Figure 5. The BF micrograph (Figure 5a) shows that SiC crystals start to form inside interfacial cracks between pitch fiber and the CVI layer. Some of the crystals are revealed in Figures 5b and 5c using DF imaging techniques which enhance the diffraction contrast.

Typical microstructure of a partially converted longitudinal pitch fiber is shown in Figure 6. The inserted SAD pattern of the partially converted fiber, Figure 6a, exhibits a mixed pattern comprising the typically strong (002) basal plane reflections and random spots from the numerous small beta-phase SiC crystals as indicated via SAD analysis. The strong (002) preferred orientation indicates that the basal planes within the unconverted portion of the pitch fiber are predominantly oriented parallel to the fiber axis. The converted fiber, i.e., the numerous SiC crystals, however, do not show any preferred orientation. As expected, the SiC crystal converted from the initially isotropic resin do not exhibit any preferred orientation, either, as shown in Figure 7.

Typical microstructure of the converted 2-D PAN/CVI C-C composite is shown in Figure 8. An example of the interface formed between unconverted and converted portions within an individual PAN fiber is depicted in Figure 8a. The mixed type SAD pattern of this region (in the insert of Figure 8a) indicates phases of both turbostratic PAN fiber and randomly oriented beta-SiC crystals. Again, the converted PAN fiber (polycrystalline SiC) does not show preferred orientation in spite of the initial strong preferred orientation exhibited by the fiber precursor. The strong preferred orientation (basal planes of substrate) inherently existing in the CVI matrix of this composite is also lost after converting into SiC, as shown in Figure 8b.

Microstructure of converted 3-D PAN/pitch C-C composite is shown in Figures 9 and 10. The fiber-matrix interface of this 3-D PAN/pitch composite is discontinuous and numerous microcracks exist along and near the fiber-matrix interface [11]. The microcracks along the interface effectively profile the fiber surface, whereas the microcracks within the matrix are formed between graphitic platelets, the broad faces of which are generally parallel to the basal planes within them.

The morphology of SiC polycrystals converted from the PAN fiber of this composite is similar to that observed in the PAN/CVI composite, as previously discussed. An example of the morphology of partially converted mesophase pitch matrix is shown in Figure 9. The pack cementation process had obviously transformed the highly graphitic mesophase pitch (see the spot pattern in Figure 9b) into a randomly oriented SiC polycrystals. Like in the other two composites, the converted SiC crystals in this 3-D PAN/pitch composite are of beta-phase, as identified by SAD analysis. The preferential conversion around the microcracks within pitch matrix is also frequently observed. An example is shown in Figure 10.

Discussion

The progress of conversion of C-C composites into SiC via pack cementation is largely affected by two microstructure-related factors: the alignment and relative amount of porosity (especially open porosity), and the relative crystallinity of various constituents in the composite. As mentioned previously, the conversion process involves two categories. The first involves a liquid-solid reaction of molten silicon with carbon, and the second involves gas-solid reaction between silicon containing vapors and carbon. Either of these mechanisms imply the important role of porosity, particularly open porosity, in the conversion process. Results of this work have indeed demonstrated this important role. For example, optical micrographs of Figures 2b, 3b, and 3b-d clearly show the extensive conversion of the porosity surrounding regions. Some of the cracks are quite deep in the composite.

Analysis of partially converted pitch/resin/CVI composite revealed that the outer (with respect to the fiber surface) CVI layers are fully converted to SiC, while the inner CVI layers remain unconverted (see Figures 2b). The inner CVI layer of this composite

consists of larger, more graphitic crystallites than the outer CVI layer [11]. The difference in the degree of crystallinity between inner and outer CVI layers is thought to lead to different degree of reactivity with silicon during pack cementation. The less graphitic CVI carbon reacts faster with silicon to form SiC and, consequently, a distinct interface is formed between the converted and the unconverted layers.

In the 3-D PAN/pitch composite, the highly graphitic mesophase pitch matrix was supposed to be the least reactive among all the components, and such a composite was supposed to undergo the least conversion. However, the results have shown that this is not true. The thickness of conversion layer in fiber bundle regions is comparable to those in the other two composites (Table 1). The conversion of interbundle matrix pockets is so severe that many matrix pockets (approximately 1 mm deep) exposed to the pack cementation environment are almost entirely converted to SiC. The reason for this is that this pitch matrix contains a large number of macroscopic and microscopic pores, which serve as short circuits for silicon diffusion. Particularly in the matrix near fiber bundles perpendicular to the free surface, the microcracks are predominantly perpendicular to the surface, which can enhance the silicon penetration to the composite interior.

Although the C-C composites chosen in this work represent different weave geometries (2-D and 3-D), different fiber-matrix combinations (pitch or PAN fibers combined with pitch, resin, or CVI matrix), different interfacial morphologies, different porosity distribution and density, and different component crystallinity, the tendency for these composites to convert to SiC during pack cementation is found to be most critically determined by their porosity and crystallinity details. The 3-D PAN/pitch composite is an example in which the porosity issue dominates the conversion process.

Conclusions

1. Some microstructural details of a series of pack cemented C-C composites, including pitch, resin, and CVI matrices reinforced with pitch or PAN fibers, are provided. The SiC crystals converted from C-C substrates are of beta-phase in all cases. Growth twins are frequently observed within SiC crystals.

2. The apparent conversion layer thickness and uniformity are largely determined by the composite type and fiber weave geometry.

3. Although the C-C composites in this study represent a wide range of varieties, the tendency for these composites to transform to SiC during pack cementation is most affected by their porosity and crystallinity details. Less graphitic phases are more prone to conversion, whereas macroporosity and microporosity always enhance conversion.

4. The carbon-SiC transformation occurs preferentially at microstructural imperfections such as micropores and microcracks and the various interfaces in the composites.

5. The converted SiC crystals are essentially equiaxed and randomly oriented, regardless of their precursor orientation, i.e., the strong preferred orientations, exhibited in fibers, mesophase pitch, and CVI are completely destroyed after converting to SiC.

Acknowledgments

The authors wish to acknowledge the Air Force Office of Scientific Research for providing the funding for this research under the contract AFOSR-88-0130. This work was also partially supported by the Materials Technology Center under the contract #6-25738.

References

1. Fitzer, E., (1987), "The Future of Carbon-Carbon Composites:, Carbon, 25, 163-190.

2. McKee, D. W. (1986), "Oxidation Behavior and Protection of Carbon-Carbon Composites," Carbon, 25, 551-557.

3. Strife, J.R. and Sheehan, J.E. (1988). "Ceramic Coatings for Carbon-Carbon Composites," Am. Ceram. Soc. Bull., 67, No. 2, 369-374.

4. McKee, D. W. (1989). "Oxidation Protection of Carbon-Carbon Composites," in Fourth Distinguished Lecture on Materials Technology, Materials Technology Center at Carbondale, Carbondale, IL.

5. Jortner, J. (1986). "Macroporosity and Interface Cracking in Multidirectional Carbon-Carbons," Carbon, Vol. 24, 603-613.

6. Jortner, J. (1977). Ju Extended Abstracts of 13th Biennial Conference on Carbon, 377-378. American Carbon Society.

7. Sheehan, J. E. (1989). "Oxidation Protection for Carbon Fiber Composites," Carbon, 27, 709-715.

8. Rogers, D. C., Scott, R. O., and Shuford, D. M. (1976). "Material Development Aspects of an Oxidation Protection System for a Reinforced Carbon-Carbon Composite," in Proceedings of the 8th National SAMPE Technical Conference, 308.

9. Rogers, D. C., Shuford, D. M., and Mueller, J. I. (1975). "Formation Mechanism of a Silicon Carbide Coating for a Reinforced Carbon-Carbon Composite," in Proceedings of the 7th National SAMPE Technical Conference, 319.

10. Marsh, H., and Smith, J. (1978). "Analytical Methods for Coal and Coal Products," Vol II, Karr, C. Jr., Academic Press, New York.

11. Ju, C. P., Tlomak, P., Stojak, J., He, J., Forrester, B., and Don, J. (1990). "TEM Characterization of C-C Composites," Proceedings of the 6th Annual Conference on Materials Technology, Materials Technology Center, Southern Illinois University, Carbondale.

Table 1

Average thickness of SiC conversion layer

C-C Composite	Thickness [microns]
2-D pitch/resin/CVI	320
2-D PAN/CVI	180
3-D PAN/pitch	430*
	1000**

Conditions: 3 hours at 1700°C; (*) fiber bundle area; (**) matrix pocket.

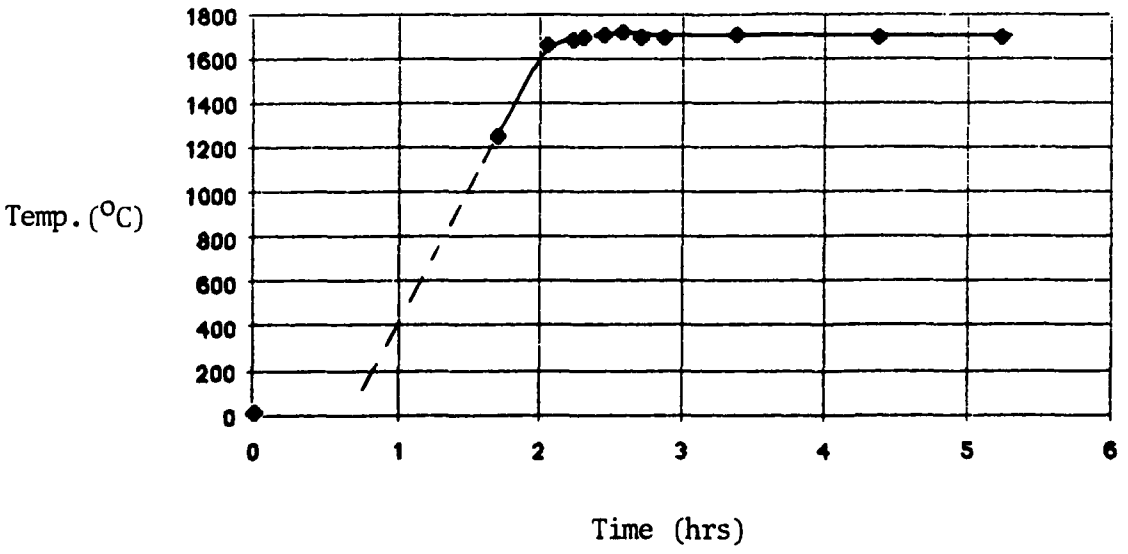

Figure 1. **Time-temperature profile for pack cementation.**

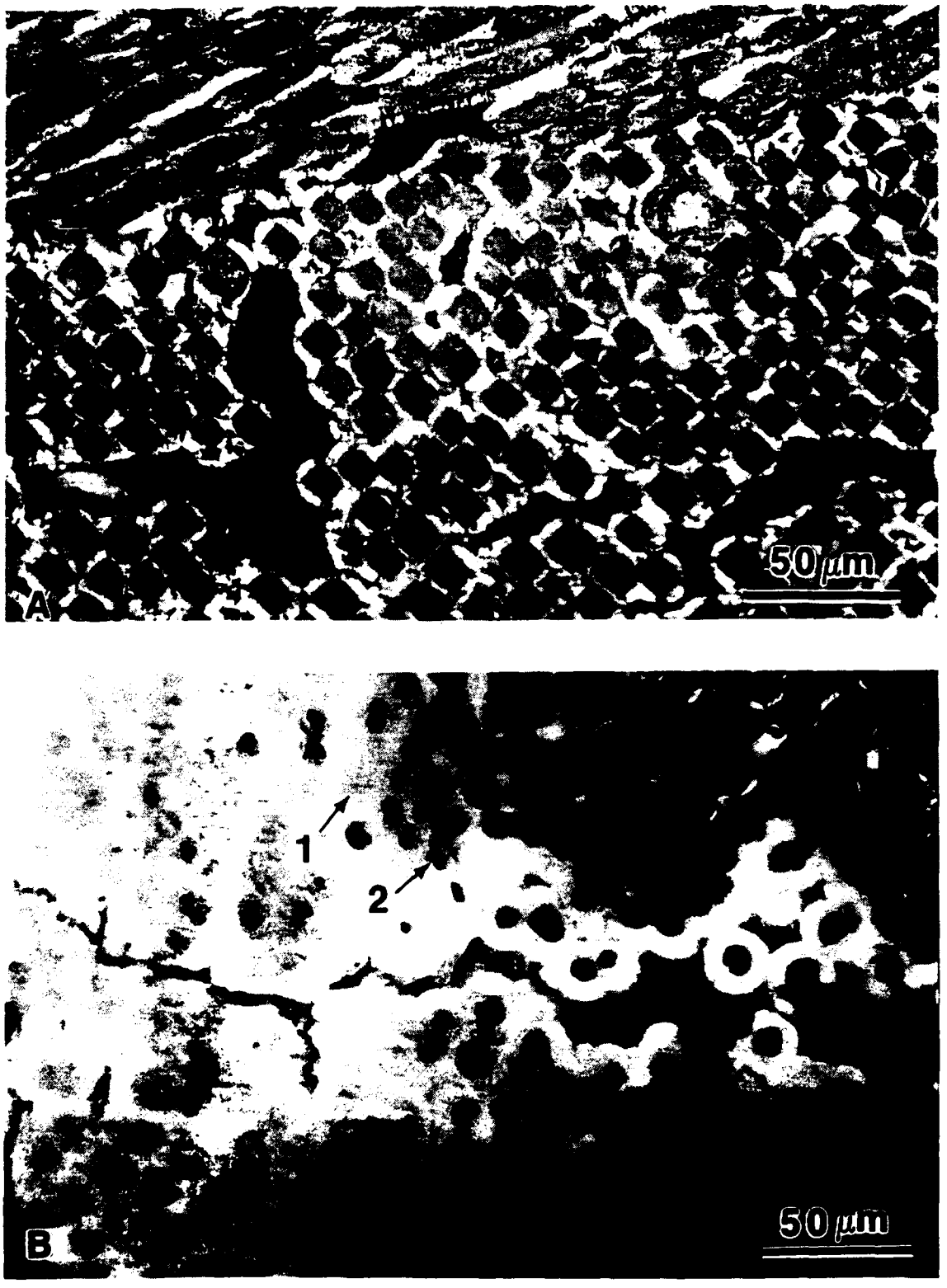

Figure 2. Polarized light micrographs showing microstructure of a transverse fiber bundle of a 2-D pitch/resin/CVI C-C composite (surface side on the left). A: as-fabricated; B: pack cemented; (1) fully converted fiber and (2) partially converted fiber.

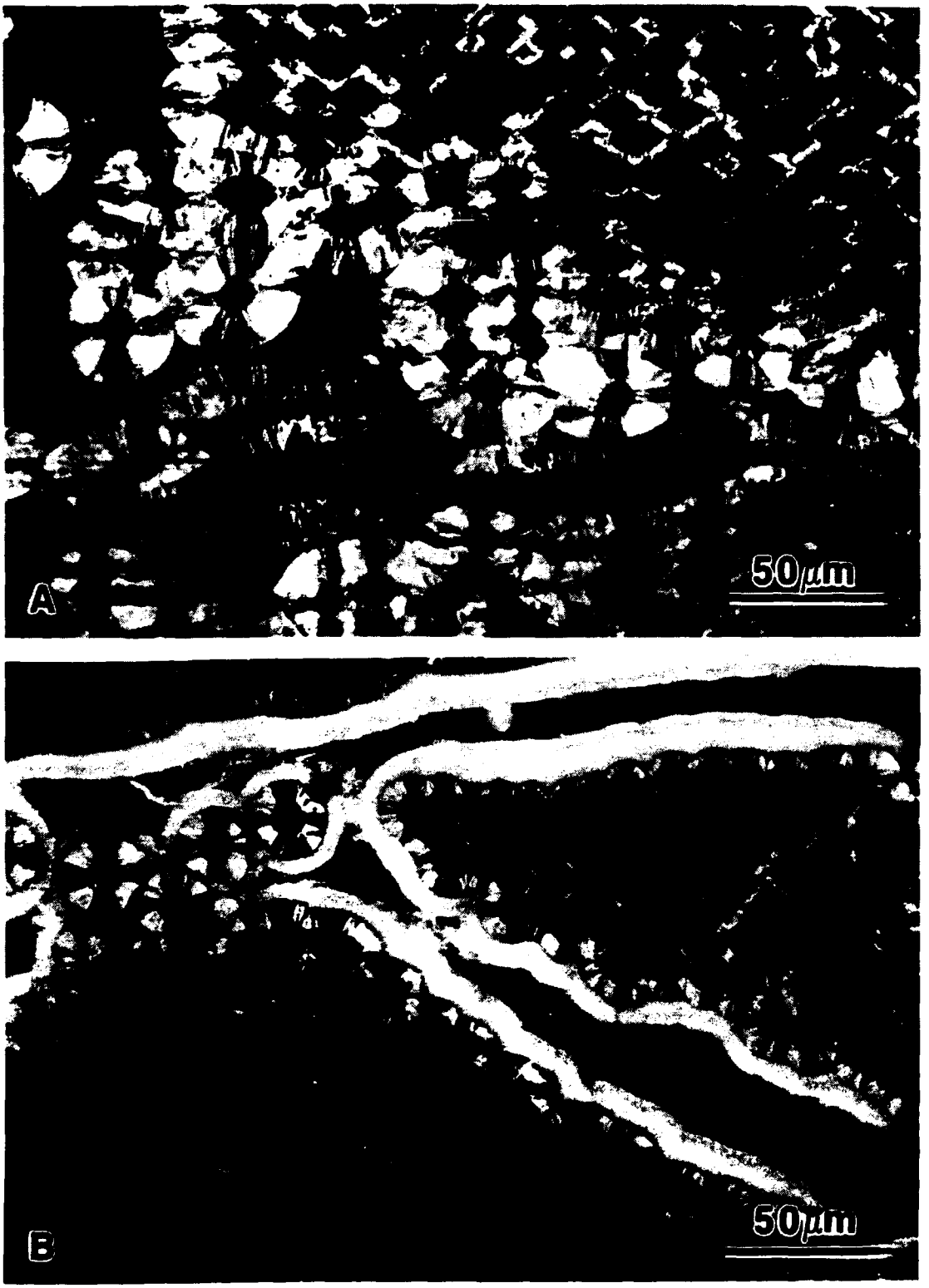

Figure 3. Polarized light micrographs showing microstructure of a transverse fiber bundle of a 2-D PAN/CVI C-C composite (surface side on the left of the micrographs). A: as-fabricated; B: pack cemented.

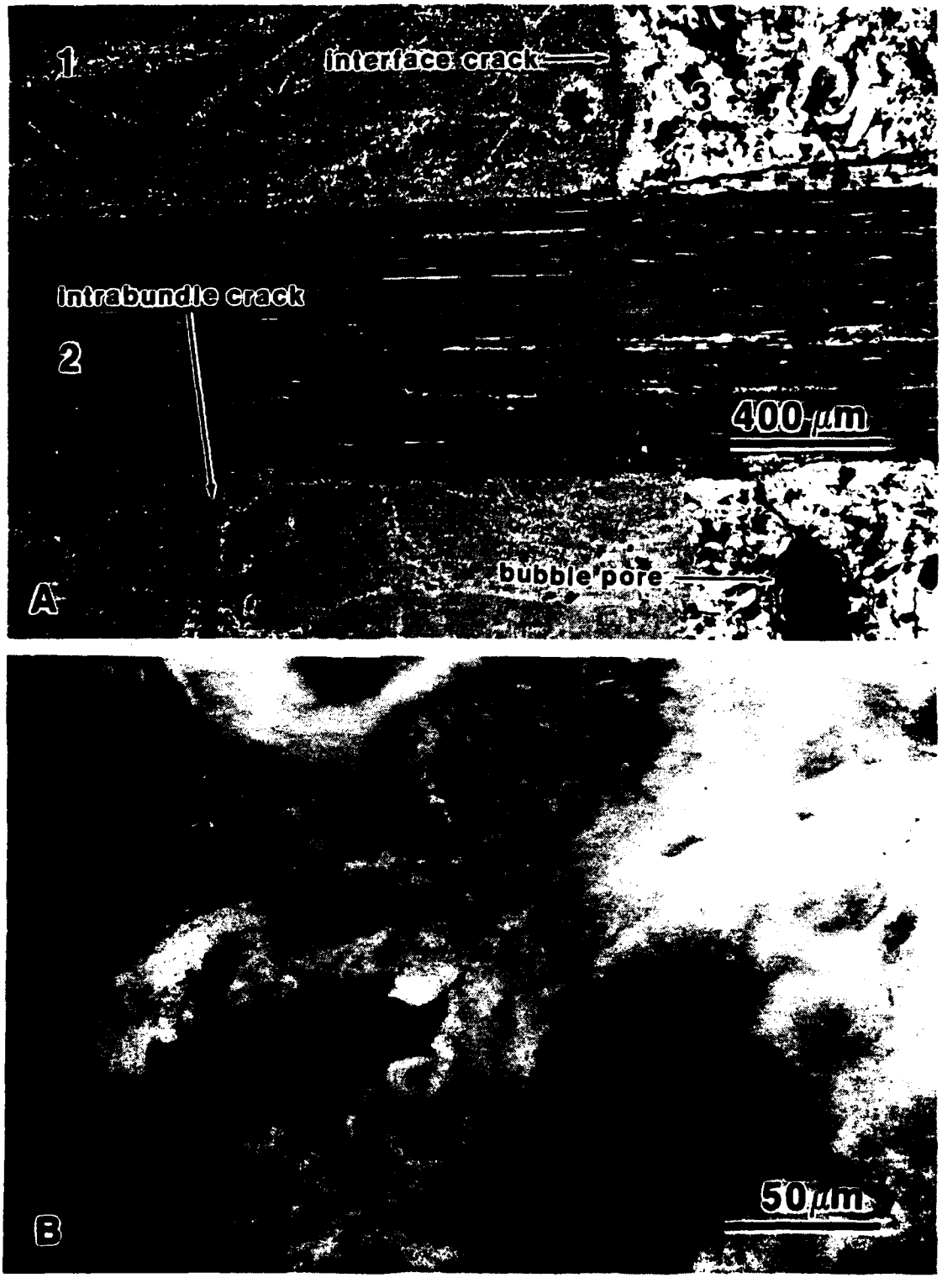

Figure 4. Polarized light micrographs of 3-D PAN/pitch C-C composite. A: cross section of orthogonal array of PAN fiber bundles in pitch matrix; (1) transverse bundle, (2) longitudinal bundle, and (3) matrix pocket. B: converted interbundle pitch matrix.

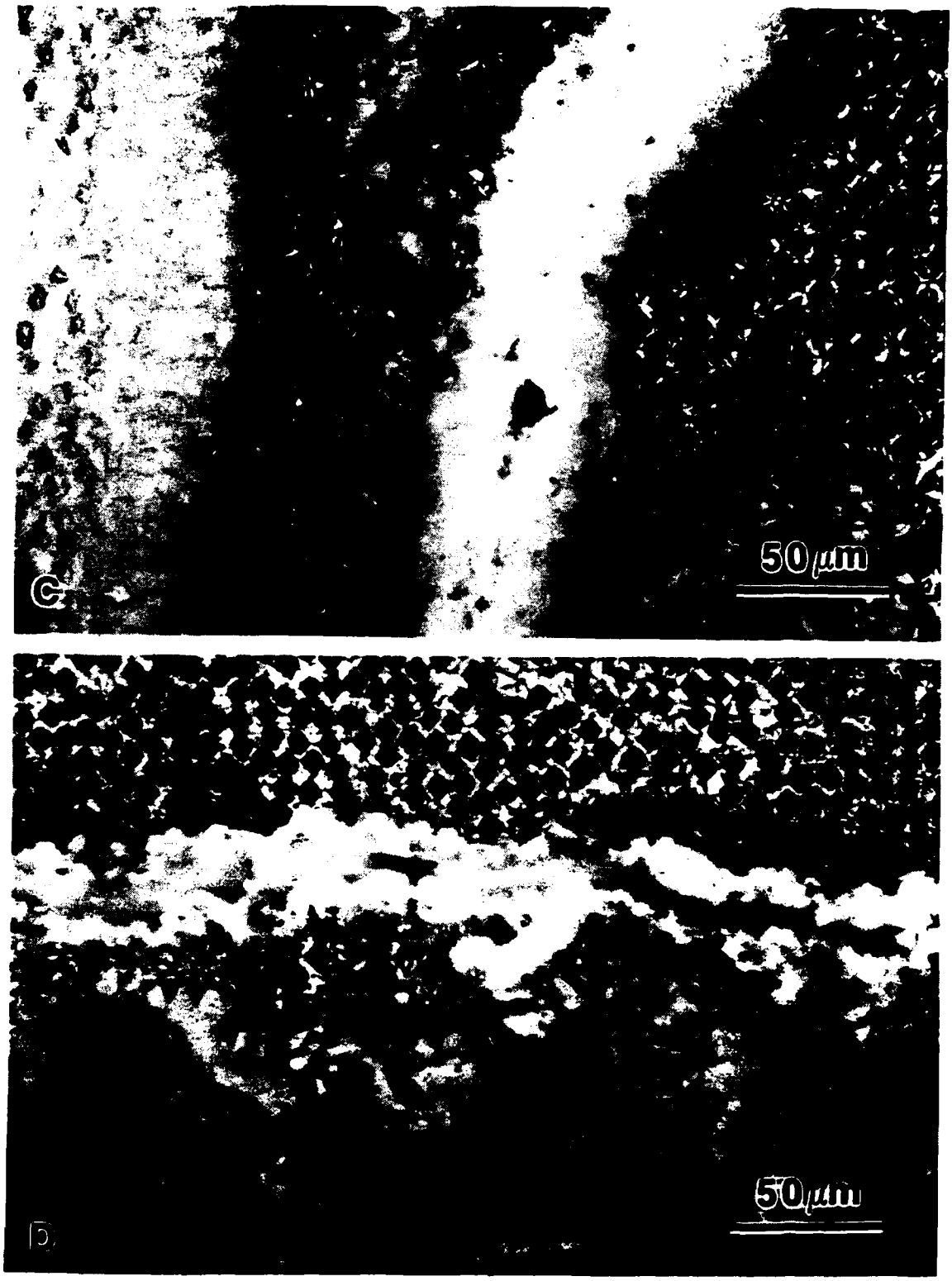

Figure 4. (Continued). C: preferential conversion in the vicinity of intrabundle crack; D: preferential conversion in the vicinity of interbundle crack.

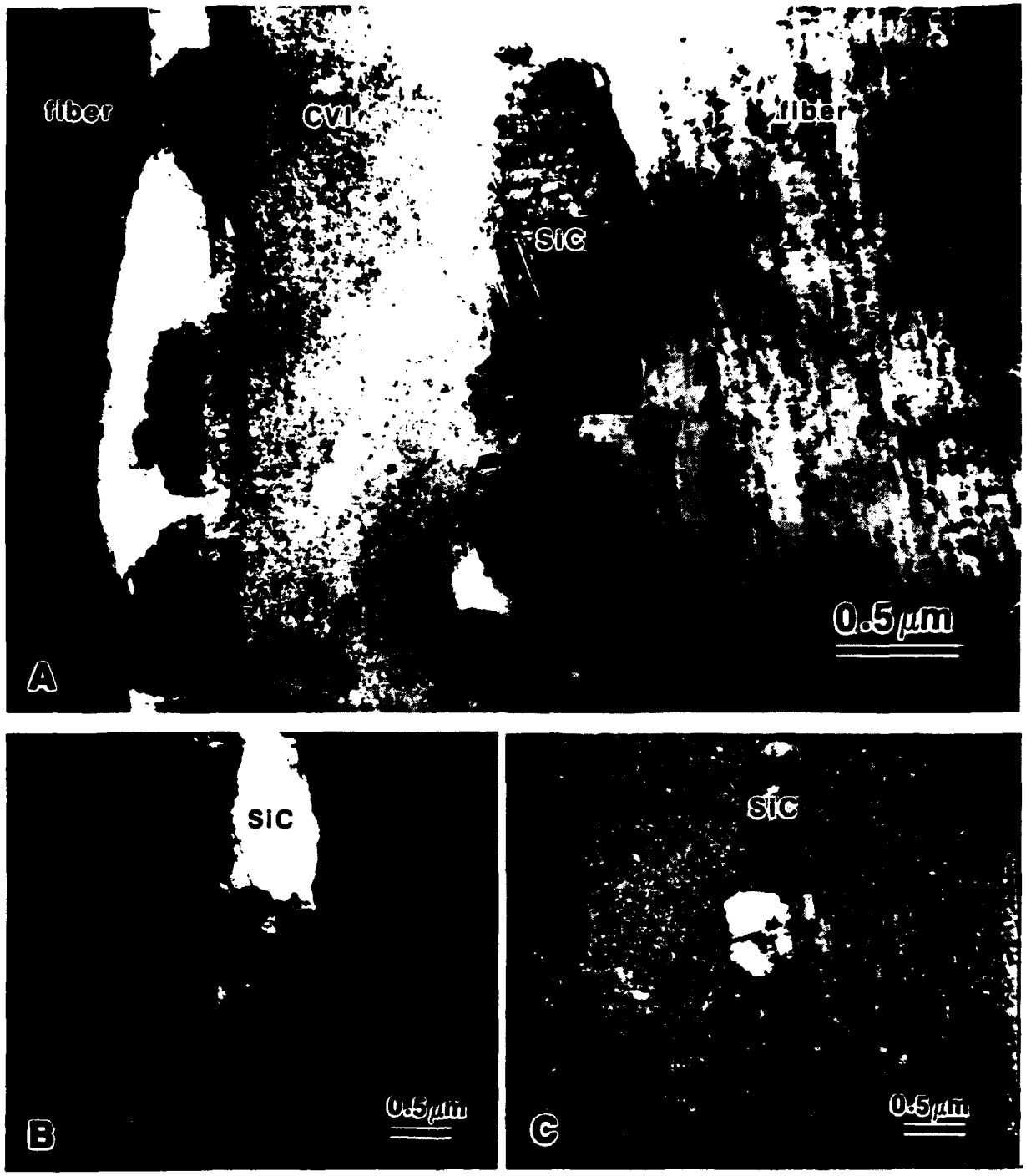

Figure 5. TEM micrographs of 2-D pitch/resin/CVI C-C composite. A: BF image of the fiber-CVI interface of converted composite; B and C: DF images of the same area using different diffracted spots.

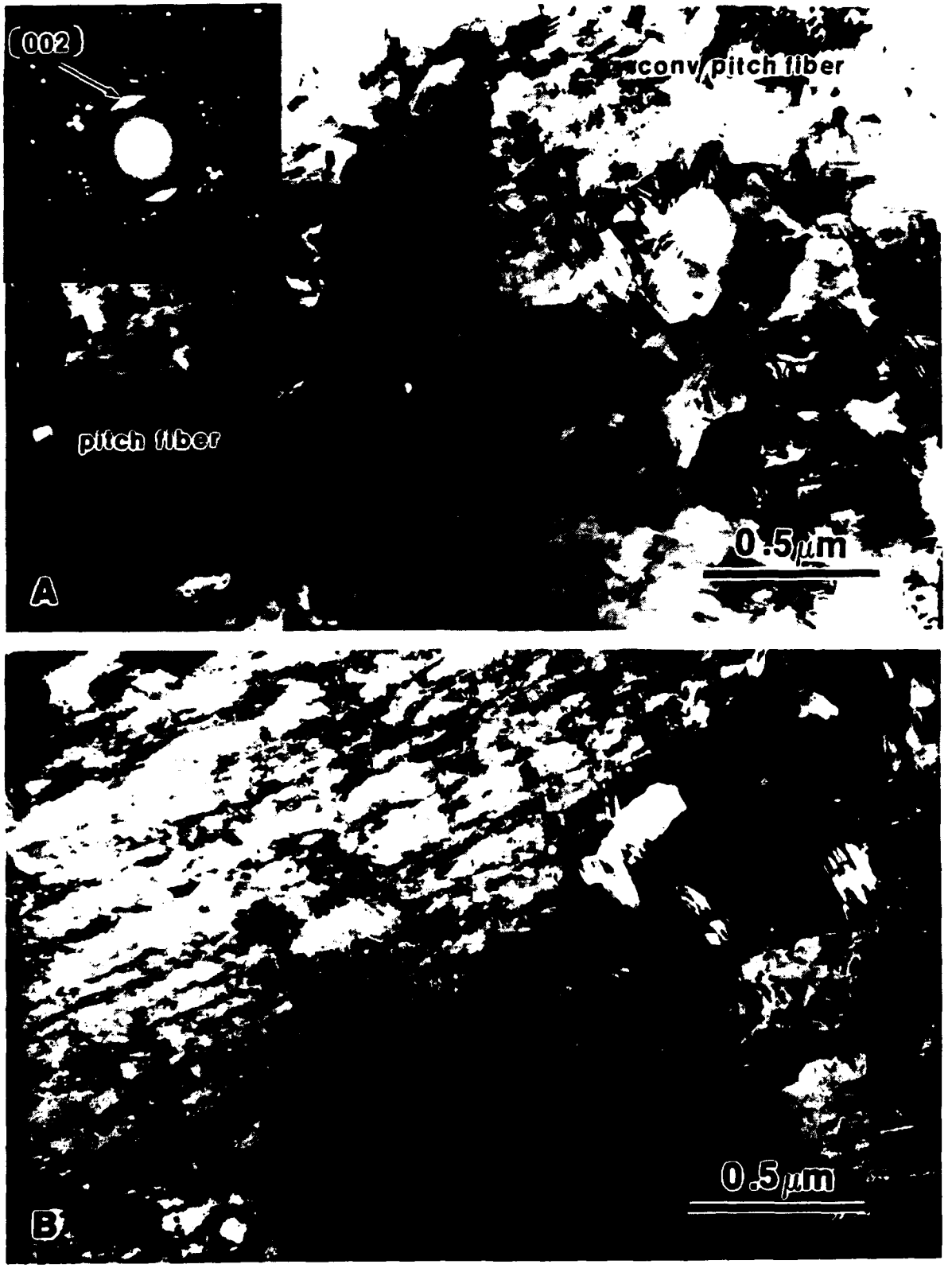

Figure 6. TEM micrographs and SAD pattern of pack cemented 2-D pitch/resin/CVI C-C composite showing a longitudinal section of a partially converted pitch fiber. A: BF image and inserted SAD pattern; B: DF image of the same area.

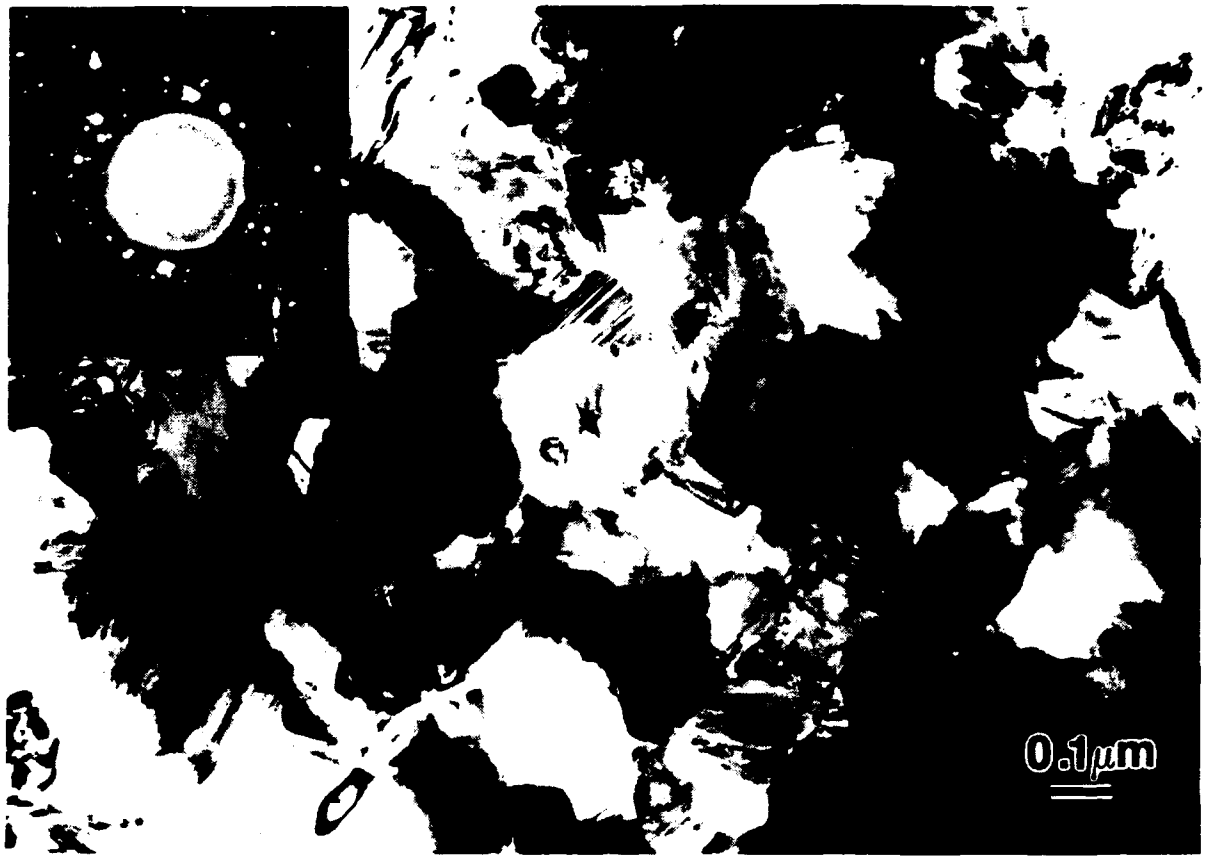

Figure 7. TEM micrograph and SAD pattern of pack cemented 2-D pitch/resin/CVI C-C composite showing an extensively converted resin matrix. The weak rings are indicative of residual unconverted resin.

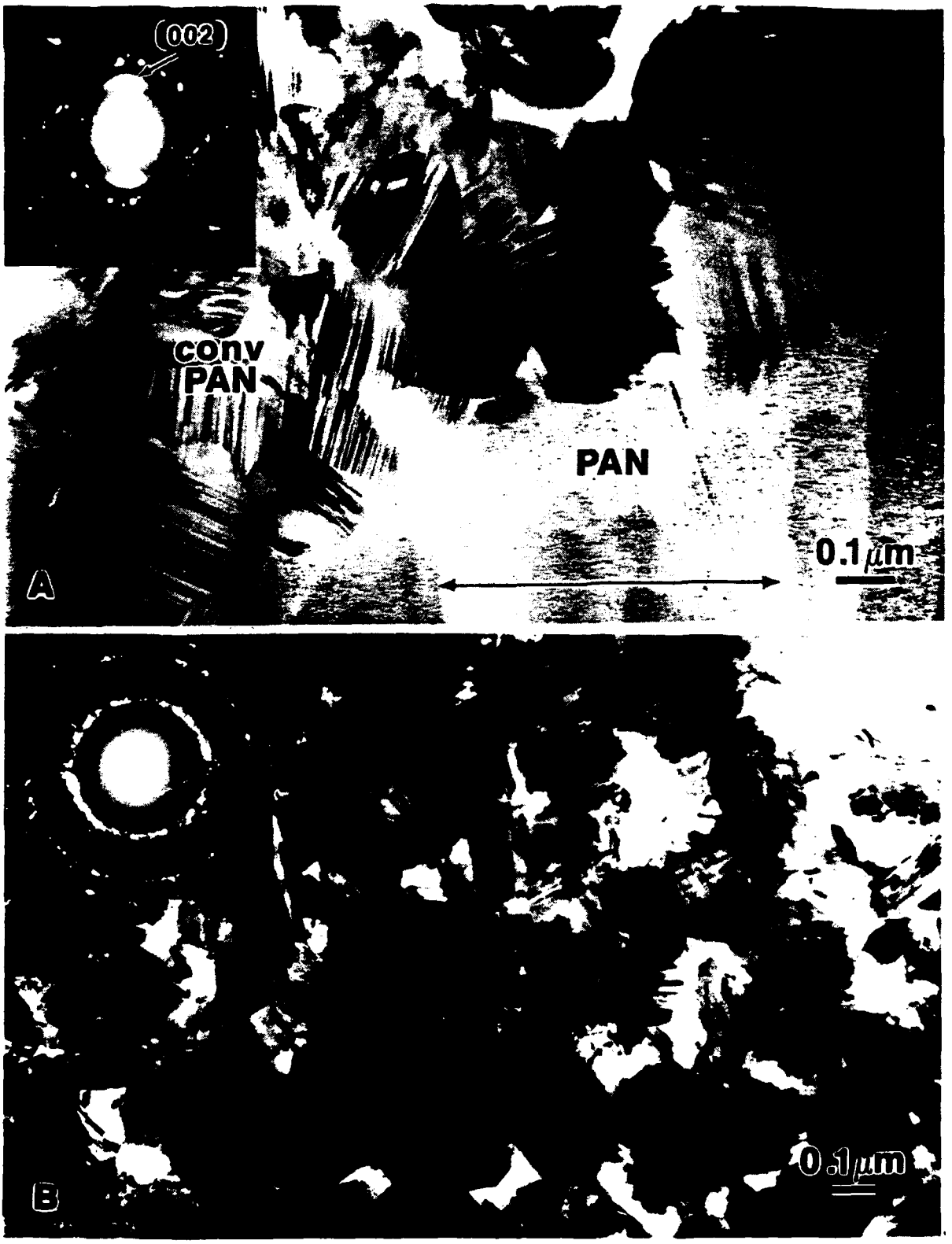

Figure 8. TEM micrographs and SAD patterns of 2-D PAN/CVI C-C composite. A: longitudinal section of a partially converted PAN fiber; arrow indicates fiber direction. B: fully converted CVI matrix.

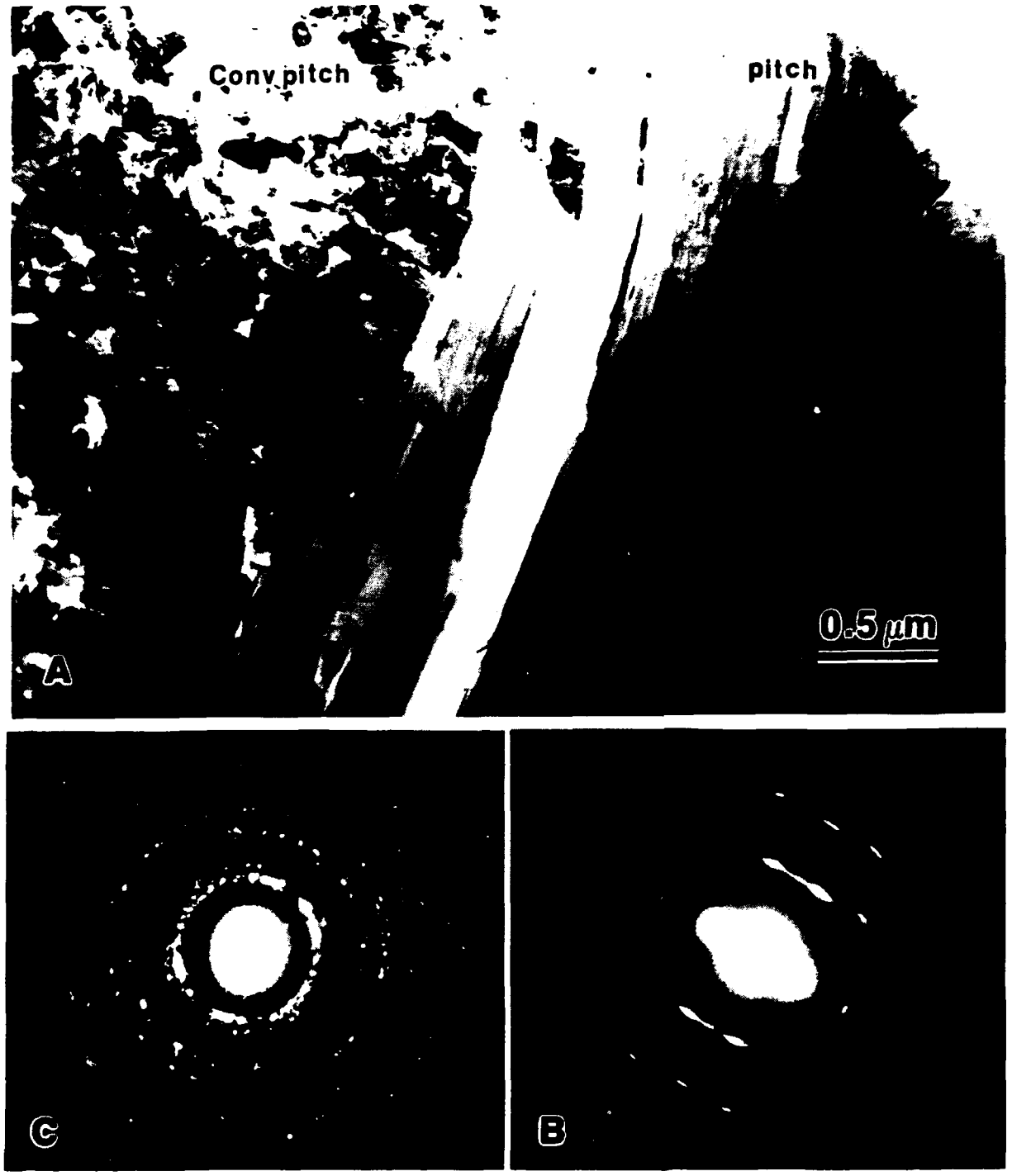

Figure 9. TEM micrograph and SAD patterns of pack cemented 3-D PAN/pitch C-C composite. A: BF image of partially converted pitch matrix; B: SAD pattern of unconverted portion C: SAD pattern of converted portion.

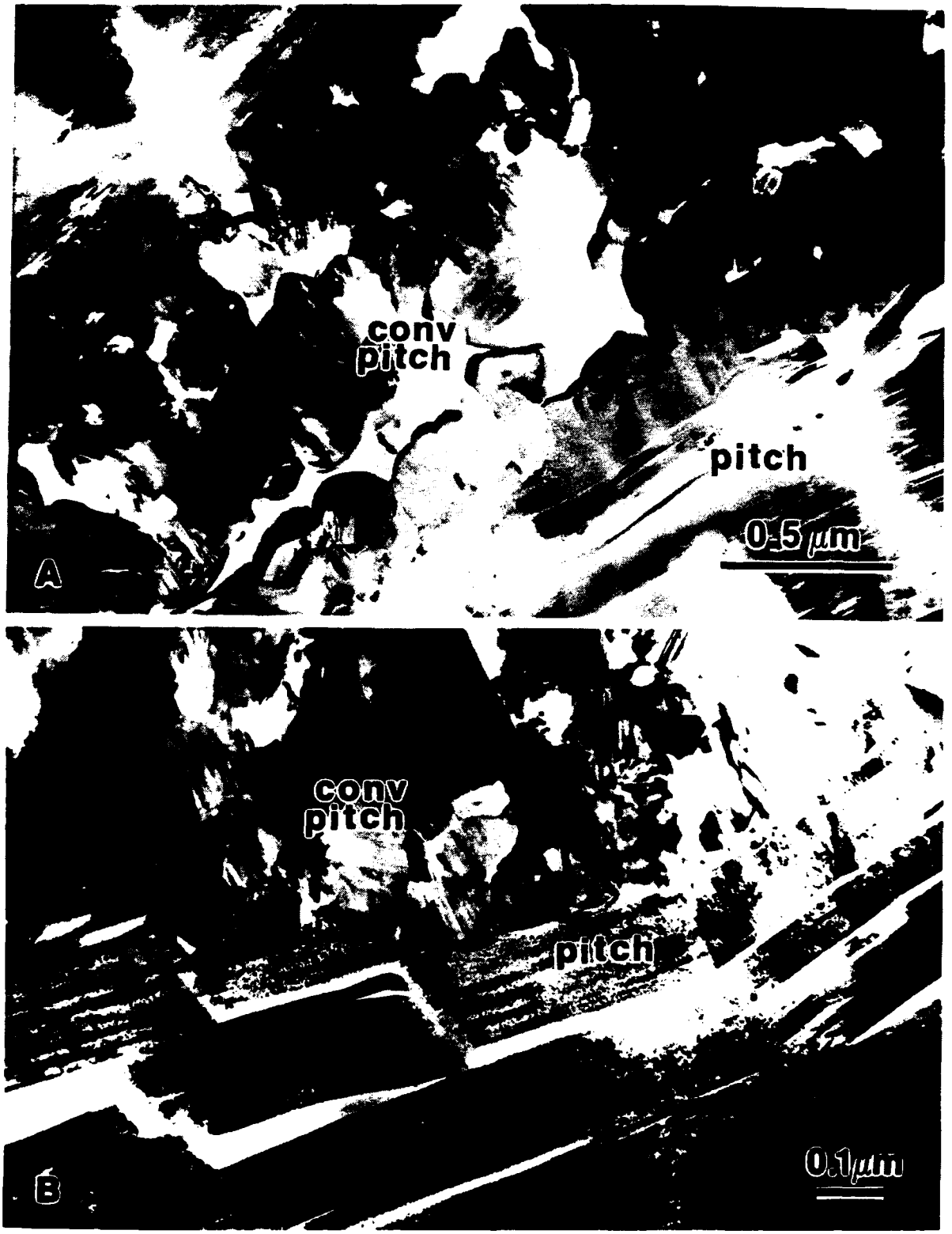

Figure 10. TEM micrographs of a 3-D PAN/pitch C-C composite. A: cross section of partially converted intrabundle pitch matrix in the vicinity of a crack; B: cross section of partially converted pitch matrix in the vicinity of intrabundle microcrack.